INSTITUTO SUPERIOR TÉCNICO
Universidade Técnica de Lisboa

Design and Control of an Electrical Machine for Flywheel Energy-Storage System

Maria Inês Lopes Marques

Dissertation submitted for obtaining the degree of
Master in **Electrical and Computer Engineering**

Jury

President: António José Rodrigues

Supervisor: Gil Domingos Marques

Members: Duarte Mesquita e Sousa

Maria José Resende

May 2008

Acknowledgements

There are many people to whom I am very grateful for their help and encouragement while undertaking the work described in this thesis. It is a pleasure to me to acknowledge them.

Firstly, I would like to especially thank my Supervisores, Prof. Gil Domingos Marques and Prof. Duarte Mesquita e Sousa, for their dedicated help, continuous support, advice and encouragement throughout this work.

The accomplishment of this work also signifies the end of five years of intense work, for that I would like to thank all the friends I have made in the different sports I have played, which were essential for keeping me sane.

I would finally like to thank all my friends, boyfriend and especially my family, in particular mum, dad, sister and grandparents, for their unconditional love, huge support and understanding when it was most required.

Abstract

Flywheel energy storage systems are now considered as enabling technology for many applications including space satellite low earth orbits, pulse power transfer for hybrid electric vehicles, and many stationary applications.

The purpose of this study is the development of a flywheel system for possible application in road vehicles. The present work reports on the design of the flywheel's rotor, the electrical machine and its control.

The flywheel's rotor was designed by calculating its dimensions, weight and material's cost for different energy capacities.

The most appropriate machine was chosen as being the Permanent Magnet Synchronous Machine, which was analyzed and the design principles calculated. The main factors that influence its design are costs, material limitations, standard specifications and special application factors.

For the machine's control, the sensorless control is desirable instead of using mechanical sensors, in order to reduce total hardware complexity, size, cost and maintenance requirements. The Direct Flux and Torque Control was chosen to control the system for the desired application.

Keywords

Flywheel energy storage system; Flywheel design; Permanent Magnet Synchronous Machine; Electrical machine design; Electrical machine sensorless control.

Resumo

Os sistemas de armazenamento de energia baseados em volantes de inércia, têm sido considerados como uma tecnologia útil em muitas aplicações, sendo usados por exemplo, como bateria em satélites de órbita terrestre baixa, como fornecedor de picos de potência em veículos híbridos eléctricos, e muitas aplicações estacionárias.

Este trabalho teve como objectivo o desenvolvimento de um volante de inércia para possível aplicação em veículos rodoviários. Seguidamente, foi feita a descrição do projecto do rotor do volante de inércia, da máquina eléctrica a utilizar e do seu controlo.

O rotor do volante de inércia foi projectado através do cálculo das suas dimensões, peso e custo dos materiais, para diferentes capacidades de armazenamento de energia.

A máquina mais apropriada para esta aplicação, foi escolhida, como sendo, a Máquina Síncrona de Ímanes Permanentes, cujos princípios de concepção foram analisados e calculados. Os principais factores que, geralmente, influenciam o projecto da uma máquina são os custos, limitações dos materiais, especificações padrão e factores relacionados com aplicações especiais.

Para o controlo da máquina, é desejável não utilizar sensores mecânicos, a fim de reduzir a complexidade total de "hardware", tamanho, custo e manutenção do sistema. O Controlo Directo do Fluxo e do Binário, foi escolhido, como sendo o sistema de controlo para a aplicação desejada.

Palavras-chave

Sistemas de armazenamento de energia baseados em volantes de inércia; Projecto de volantes de inércia; Máquina Síncrona de Ímanes Permanentes; Projecto de máquinas eléctricas; Controlo de máquinas eléctricas sem sensores mecânicos.

Table of Contents

List of Figures

List of Tables

List of Acronyms

AC	Alternate Current
AFPM	Axial-Flux Permanent Magnet Machine
back e.m.f.	Open-circuit voltage induced in a stator winding due to the magnets
DC	Direct Current
DSP	Digital Signal Processor
EU	European Union
HVF	Harmonic Voltage Factor
IEC	International Electrotechnical Commission
IEEE	Institute of Electrical and Electronics Engineers
IPMSM	Interior Permanent Magnet Synchronous Machine
m.m.f.	Magnetomotive Force
NASA	National Aeronautics and Space Administration
NEMA	National Electrical Manufacturers Association
PI	Proportional Integral
PM	Permanent Magnet
PMSM	Permanent Magnet Synchronous Machine
PV	Photovoltaic
PWM	Pulse Width Modulation
RFPM	Radial-Flux Permanent Magnet machine
RMS	Root Mean Square
SMES	Superconducting Magnetic Energy Storage
SPMSM	Surface Permanent Magnet Synchronous Machine
UPS	Uninterruptible Power Supply
VSI	Voltage Source Inverter
y-connection	Star-connection

List of Symbols

Latin Symbols:

A	Specific electric loading [ampere-conductors per metre]
a	Relation between the inner radius and the outer radius, $a = \frac{r_i}{r_o}$
B_{gav}	Average air gap flux density, also known as specific magnetic loading [Wb/m^2]
c	Constant
$\cos\varphi$	Power factor
D	Diameter of the stator bore [m]
D_{in}	Inner diameter of the stator bore [m]
D_{out}	Outer diameter of the stator bore [m]
E	Kinetic energy stored [J]
E_{MJ}	Kinetic energy stored [MJ]
E_{lim}	Energy limit [MJ]
$E_{lim\_per\_volume}$	Energy limit per total volume [MJ/m^3]
$E_{\lim\_per\_volume\_mass}$	Energy limit per total volume of rotating mass [MJ/m^3]
e_m	Kinetic energy per unit mass [J/kg]
E_{ph}	RMS voltage induced in the entire phase winding [V]
e_v	Kinetic energy per unit volume [J/m^3]
f	Frequency [Hz]
G_a	Switching function, a
G_b	Switching function, b
G_c	Switching function, c
h	Length of the flywheel's cylinder [m]
I	Moment of inertia [Kg/m^2]
I_{ph}	Current in the entire phase winding [A]
i_s	Amplitude of the stator winding current [A]
$\lvert \bar{i}_{sref} \rvert$	Modulus of the reference stator-current space vector [A]
i_{sD}	D component of the stator winding current [A]
i_{sQ}	Q component of the stator winding current [A]

K	Shape factor
K_w	Winding factor
L	Active length of the core [m]
L_s	Amplitude of the stator winding inductance [H]
L_{sD}	D component of the stator winding inductance [H]
L_{sQ}	Q component of the stator winding inductance [H]
m	Mass [Kg]
M_{em}	Electromagnetic torque [Nm]
N	Speed [rpm]
N_{ph}	Number of conductor turns
p	Number of poles
P_{kW}	Active power [kW]
P_n	Rated Motor Power [W]
q	Number of stator slots
r	Flywheel radius [m]
r_i	Inner radius [m]
r_o	Outer radius [m]
R_s	Stator winding resistance [Ω]
s	Laplace operator
S	Rated Slip [%]
S_{kVA}	Apparent power [kVA]
T	Time constant
U_d	D.C. link voltage [V]
u_s	Amplitude of the stator winding voltage [V]
u_{s3}	Third-harmonic voltage [V]
u_{sD}	D component of the stator winding voltage [V]
u_{sQ}	Q component of the stator winding voltage [V]
Greek Symbols:	
ε_{yy}	Transverse strain [Pa]
ε_{xx}	Longitudinal or axial strain [Pa]
ϕ_p	Flux linkage of the coil [Wb]
η	Machine's efficiency [%]
λ	Slot pitch [m]
ν	Poisson ratio
π	Constant with the value of 3.14159265

ρ	Density of the cylinder's material [Kg/m^3]
ρ_s	Stator position angle [rad]
σ	Maximum stress in the flywheel's material [MPa]
σ_r	Radial stress [MPa]
σ_t	Tangential stress (also known as hoop stress) [MPa]
τ	Pole pitch [m]
υ	Peripheral velocity [m/s]
ω	Angular velocity [rad/s]
ω_b	Base speed [rad/s]
ω_{max}	Maximum speed [rad/s]
ω_r	Rotor speed [rad/s]
ψ_{r3}	Third-harmonic rotor flux [Wb]
ψ_s	Amplitude of the stator flux linkage [Wb]
ψ_{sD}	D component of the stator flux linkage [Wb]
ψ_{sQ}	Q component of the stator flux linkage [Wb]
ψ_{sf}	Rotor flux linkage generated by the permanent magnets [Wb]

List of Programmes

FEMM

MATLAB *MATLAB is a registered trademark of the MathWorks, Inc.

MATLAB
Simulink

Chapter 1

Introduction

This chapter gives a brief overview of the work. Before establishing work targets, the scope and motivations are brought up. The current State-of-the-Art in relation to the scope of the work is also presented. At the end of the chapter, the work structure is provided.

1.1 Scope of the work

The high price of fossil energy in the earliest 21st century increased the demand for new alternatives to power vehicles and other applications. This was the main driving force for the study and design of a flywheel for possible application in electric vehicles.

A flywheel is a mechanical battery, represented in figure 1.1, that typically consists of a high speed inertial composite rotor to store kinetic energy, a magnetic bearing support and control system, an electrical machine that can run either as a motor or a generator to undertake the energy transfer to and from the flywheel, a vacuum support housing and containment, compact heat removal and exchangers, instrumentation monitoring and control, and power electronics for electrical conversion.

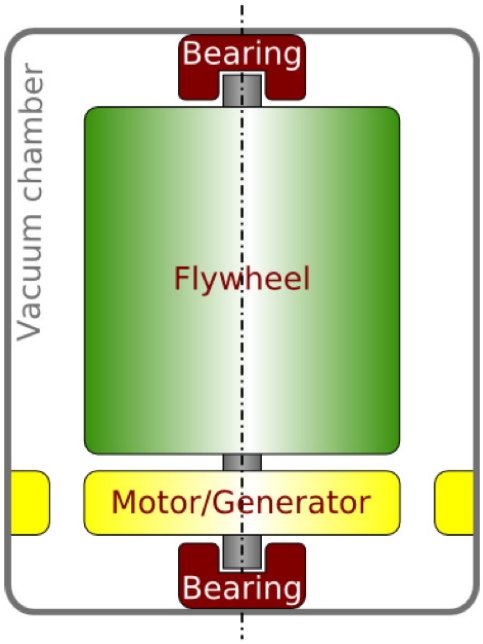

Figure 1.1. Schematic view of the flywheel's storage system. [24]

The design life has no degradation during its entire cycle life unlike chemical batteries. A flywheel can discharge cyclically to zero energy without any degradation whatsoever, unlike the failings of all chemical batteries.

Flywheel energy storage systems are attractive for the types of applications for which a designer might also consider conventional electrochemical batteries or superconducting magnetic energy storage (SMES).

Table 1.1. Flywheel battery comparison with Lead-Acid and Superconducting battery types. [23]

How Flywheel Batteries Compare to Lead-Acid and Superconducting Types

	Lead-acid battery	Flywheel battery	SMES
Storage mechanism	Chemical	Mechanical	Electrical
Life (years in service)	3–5	>20	~20
Technology	Proven	Promising	Promising
Number of manufacturers	~ 700	~ 10	~1
Annual sales (in US $millions)	~ 7000	~ 2	A few
Temperature range	Limited	Less limited	Controlled
Environmental concerns	Disposal issues	Slight	Slight
Relative size (equivalent power/energy)	Larger	Smallest	In between
Practical time to hold a charge	Years	Hours	Days
Price, per kilowatt	$50–$100	$400–$800	>$300

SMES = Superconducting magnetic energy storage.

Source: University of Texas

1.2 State of art in relation to the scope of the work

The origins and use of flywheel technology for mechanical energy storage began several decades ago and was developed throughout the Industrial Revolution. The next big milestones were durprassing the 1960s and 1970s when NASA sponsored programs proposing energy storage flywheels as possible primary sources for space missions. However,

it was not until the 1980's when microelectronics, magnetic bearing systems and high power density motor-generators became enabling technologies. The next decade proved that a mechanical battery (flywheel) could be better than chemical batteries in many applications.

Flywheel energy systems are now considered as enabling technology for many applications including space satellite low earth orbits, pulse power transfer for hybrid electric vehicles and many other applications.

Projections of flywheel energy storage technology into the 21st Century shall advance by more inexpensive and stronger fiber materials and resin systems. Increases in tensile modulus also improve system performance with stiffer rotors and housing structures. This is significant, since energy density is proportional to tensile strength. The cost and performance of magnetic bearing technology is advancing flywheel systems with lower operational power, higher load capacity, and faster response.

1.3 Thesis outline

This thesis reports the study and design of an electrical machine (and its control) for application on a flywheel energy-storage system, for possible application at road vehicles. This system could be applied as power peaking, in hybrid vehicles, or as energy storage, in electric vehicles.

Chapter 2 describes the rotor's theoretical fundamentals and the calculations for its dimensions, weight and material's cost.

An important limitation for the flywheel design are the stress forces, which are limited according to the materials applied at the rotor. A study of the relation between the outer and inner radius and the stress forces will be used to dimension the rotor piece.

Chapter 3 describes briefly the different electrical machines for possible application at a flywheel and presents a study of the work performed up to date. After this study it is possible to choose the most appropriate machine to use at the previously designed flywheel.

Having the flywheel designed and the machine type chosen, Chapter 4 analyses and calculates the design principles of the machine. There are some factors influencing the design, which are costs, material limitations, standard specifications and special application factors.

The major issues in designing a flywheel, may be divided into 5 areas: electrical, magnetic, insulation, thermal and mechanical designs.

The stress forces at the machine's rotor must be studied in order to guarantee that the materials used on the rotating mass, that supports the machine, have the strength to hold the stresses.

Chapter 5 reports on the machine sensorless control.

Using the results of the flywheel's rotor and electrical machine design, a study of the sensorless control methods is performed.

A sensorless control is desirable instead of using mechanical sensors, in order to reduce total hardware complexity, size, cost and maintenance requirements.

Finally, after the control principles and methods are studied, the best and most efficient control system can be chosen for the desired application.

1.4 Conclusions

In this dissertation, several aspects of flywheels are analysed. To illustrate the presentation, a practical case was considered: a flywheel of 5kWh capacity and 30 kW for application in an electrical vehicle.

The chosen flywheel's rotor material was the carbon based fibers, because they allow a less heavy rotor and with the ability to sustain much higher speeds and energy, comparing to iron and other classical materials.

The transformation between rotational kinetic energy and electrical energy was performed with a permanent magnet synchronous machine that was chosen taking into

account its efficiency, smaller size and easier control, when compared to direct current machines or induction machines.

For the machine's control, the sensorless control is desirable instead of using mechanical sensors, in order to reduce total hardware complexity, size, cost and maintenance requirements. Due to its efficiency and simplicity, the Direct Flux and Torque Control, was the chosen technique.

Possible future developments of the work described in this thesis, could be the practical implementation of the chosen control system, the construction of the designed flywheel and the posterior application of the designed machine at this flywheel.

Chapter 2

Flywheel Design Principles

This chapter provides an overview over the design principles of a flywheel energy-storage system for road vehicles. The flywheel has a rotor; this rotor is an object that rotates at a certain speed with a certain mass that will store energy by its speed and mass. The rotor that can also be called the wheel, has been composed, in the past, by iron and other classical materials but new discoveries in engineering with carbon based fibers will make the wheel less heavy and with the ability to sustain much higher speeds. This issue will be further discussed in this chapter, which focuses on the design fundamentals of the wheel.

2.1 Introduction

From the high price of fossil energy in the early 21st century, came the conclusion that it is necessary to find another way to power vehicles and other applications. Flywheels may be a good solution but a first study of their shape and mass is required to have a better view of its applications. Another important factor is the speed; there must be a balance between speed, mass and size, which is expressed in order to flywheel's rotor outer radius.

Another problem in the design of the flywheel is the materials used on the rotating mass. It's known that materials like iron and other classic materials don't have the strength to hold high rotation speeds. The solution may be the new carbon composite materials due to their higher resistance to twist forces comparing to iron and other classic materials.

2.2 Theoretical approach of flywheel's rotor design

2.2.1 Design fundamentals

- *Fundamental equations:*

The energy storage in a flywheel system is given by the equation (2.1), where E is the kinetic energy stored, I is the moment of inertia and ω the angular velocity of the flywheel.

$$E = \frac{1}{2} \cdot I \cdot \omega^2 \tag{2.1}$$

The moment of inertia is a function of its shape and mass, given by equation (2.2)

$$dI = m \cdot r^2 \tag{2.2}$$

For the common solid cylinder, the expression for I is given on equation (2.3), where h is the length of the cylinder, r is the radius and ρ is the density of the cylinder's material.

$$I = \frac{1}{2} \cdot r^4 \cdot \pi \cdot h \cdot \rho \tag{2.3}$$

The other dominating shape is a hallow circular cylinder, approximating a composite or steel rim attached to a shaft with a web, that results in equation (2.4).

$$I = \frac{1}{2} \cdot \pi \cdot h \cdot \rho \cdot \left(r_o^4 - r_i^4 \right) \tag{2.4}$$

Where r_o is the outer radius and r_i is the inner radius.

Then, in equation (2.5), there is the energy (in [*MJ*]) that can be stored in a flywheel system in function of its speed and inner and outer radius.

$$E_{MJ} = \frac{1}{4} \cdot \pi \cdot h \cdot \rho \cdot \left(r_o^4 - r_i^4 \right) \cdot \omega^2 \tag{2.5}$$

As a result of equation (2.1), the most efficient way to increase the energy stored in a flywheel is to speed it up. However, there is a problem with this solution, the materials that compose the wheel of that rotating system will limit the speed of the flywheel, due to the stress developed, called tensile strength, σ.

- *Analysis of stress forces:*

The analysis of the stress forces is an important factor in the wheel's dimensioning. The tensile strength of a rotation system is composed by two kinds of forces, the radial and the tangential stresses, respectively σ_r and σ_t.

By considering a wheel with uniform thickness and density ρ (figure 2.1), the centrifugal force, dF_c, acting on an element, dm, of the disc can be written as follows [32]:

$$dF_c = dm \cdot r \cdot \omega^2 = \rho \cdot h \cdot r^2 \cdot d\varphi \cdot dr \cdot \omega^2 \tag{2.6}$$

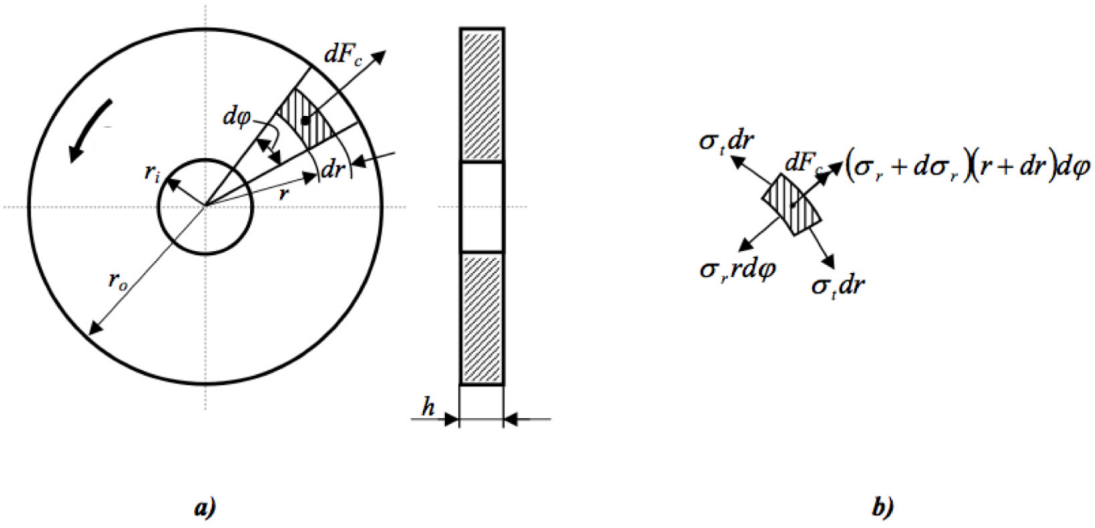

Figure 2.1. Forces and constraints in a wheel with uniform thickness. [32]

By considering the separate element of the disc (figure 2.1.b), the following relation was obtained [32]:

$$(\sigma_r + d\sigma_r) \cdot (r + dr) \cdot d\varphi - \sigma_r \cdot r \cdot d\varphi - 2 \cdot \sigma_t \cdot dr \cdot \sin\frac{d\varphi}{2} + \rho \cdot h \cdot r^2 \cdot d\varphi \cdot \omega^2 = 0 \tag{2.7}$$

From figure 2.1 and equation (2.7) it was possible to obtain the stresses, for a hollow cylinder with an isotropic material. The radial stress is represented by equation (2.8) and the tangential stress (also known as hoop stress) is represented by equation (2.9) [5, 32].

$$\sigma_r(r) = \frac{3+v}{8} \cdot \rho \cdot \omega^2 \cdot \left(r_o^2 + r_i^2 - \frac{r_o^2 \cdot r_i^2}{r^2} - r^2 \right) \tag{2.8}$$

$$\sigma_t(r) = \frac{3+v}{8} \cdot \rho \cdot \omega^2 \cdot \left(r_o^2 + r_i^2 + \frac{r_o^2 \cdot r_i^2}{r^2} - \frac{1+3 \cdot v}{3+v} \cdot r^2 \right) \tag{2.9}$$

Where *v* is the Poisson ratio, which is a constant of the material of the rotor (this ratio is described in Annex 1).

The next figure shows an example intended to help the understanding of the radial and tangential stresses.

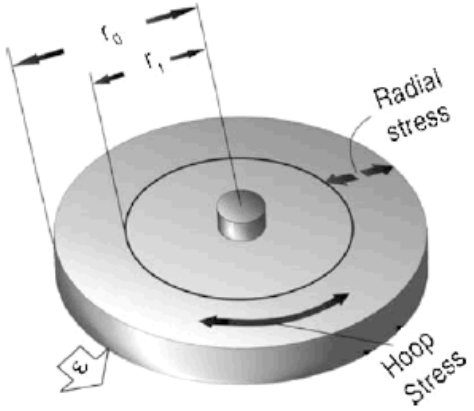

Figure 2.2. Radial and tangential stress in a short hollow cylinder rotating about its axis with angular velocity ω. [5]

2.2.2 Inner radius, outer radius and rotation speed relations

In order to dimension the rotor piece, a study of the relation between the outer radius and the inner radius and the stress forces relationship is required to dimension the wheel.

Using equations (2.8) and (2.9), the radial and tangential stress tensions in order to $\frac{r_i}{r_o}$ can be achieved by:

$$\sigma_r = \frac{3+v}{8}\cdot\rho\cdot\omega^2\cdot\left(r_o^2+r_i^2-\frac{r_o^2\cdot r_i^2}{r^2}-r^2\right)=\frac{3+v}{8}\cdot\rho\cdot\omega^2\cdot r_o^2\cdot\left(1+\frac{r_i^2}{r_o^2}-\frac{r_i^2}{r_o^2}\cdot\frac{r_o^2}{r^2}-\frac{r^2}{r_o^2}\right)\Leftrightarrow$$

$$\Leftrightarrow\frac{\sigma_r}{\rho\cdot\omega^2\cdot r_o^2}=\frac{3+v}{8}\cdot\left(1+\frac{r_i^2}{r_o^2}-\frac{r_i^2}{r^2}-\frac{r^2}{r_o^2}\right) \qquad (2.10)$$

$$\sigma_t = \frac{3+v}{8}\cdot\rho\cdot\omega^2\cdot\left(r_o^2+r_i^2+\frac{r_o^2\cdot r_i^2}{r^2}-\frac{1+3\cdot v}{3+v}\cdot r^2\right)\Leftrightarrow\frac{3+v}{8}\cdot\rho\cdot\omega^2\cdot r_o^2\cdot\left(1+\frac{r_i^2}{r_o^2}+\frac{r_i^2}{r^2}-\frac{1+3\cdot v}{3+v}\cdot\frac{r^2}{r_o^2}\right)\Leftrightarrow$$

$$\Leftrightarrow\frac{\sigma_t}{\rho\cdot\omega^2\cdot r_o^2}=\frac{3+v}{8}\cdot\left(1+\frac{r_i^2}{r_o^2}+\frac{r_i^2}{r^2}-\frac{1+3\cdot v}{3+v}\cdot\frac{r^2}{r_o^2}\right) \qquad (2.11)$$

Using equations (2.10) and (2.11) and setting $\frac{r}{r_0}$ with different values, a study was performed regarding the values of $\frac{\sigma_t}{\rho\cdot\omega^2\cdot r_o^2}$ and $\frac{\sigma_r}{\rho\cdot\omega^2\cdot r_o^2}$, represented in the next graphic, considering $a=\frac{r}{r_0}$.

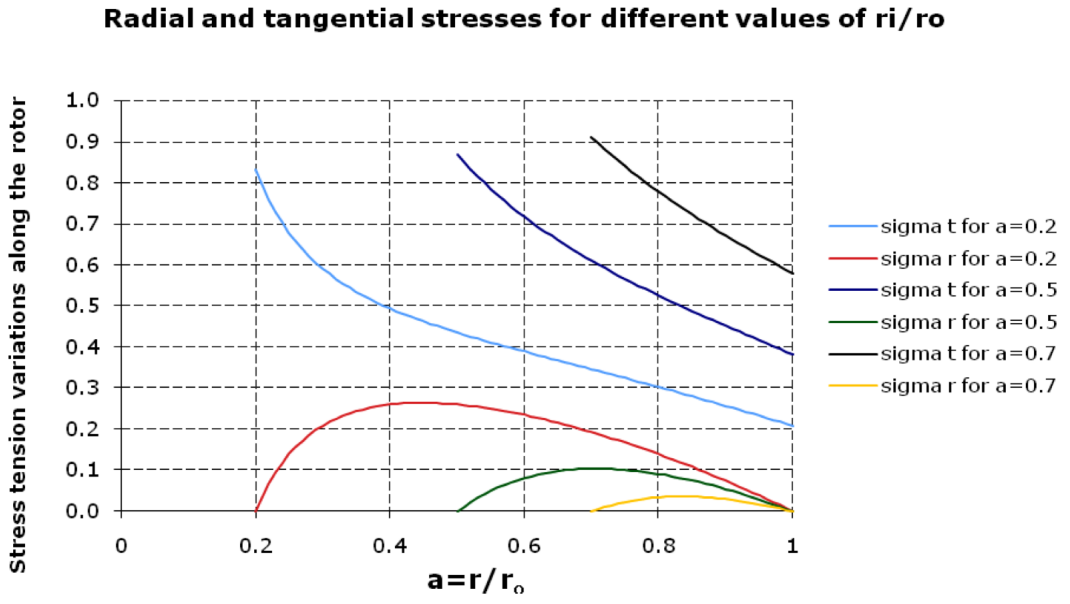

Figure 2.3. Stress tension variations along the rotor for *a*=0.2; *a*=0.5 and *a*=0.7.

Looking at the variation of $\frac{r}{r_o}$, it can be concluded that the tangential stress is always more important than the radial stress, which makes the tangential stress the most critical one.

As it was shown in figure 2.3, the maximum of the tangential stress is approximately 1, which yields in equation $\frac{\sigma_t}{\rho \cdot \omega^2 \cdot r_o^2} \approx 1$.

For a limited σ_t, of σ_t=*825MPa* (which is half of the maximum admitted, for security reasons), the outer radius and the rotation speed are related and when the outer radius is chosen, the flywheel speed is limited, as the next graphic expresses.

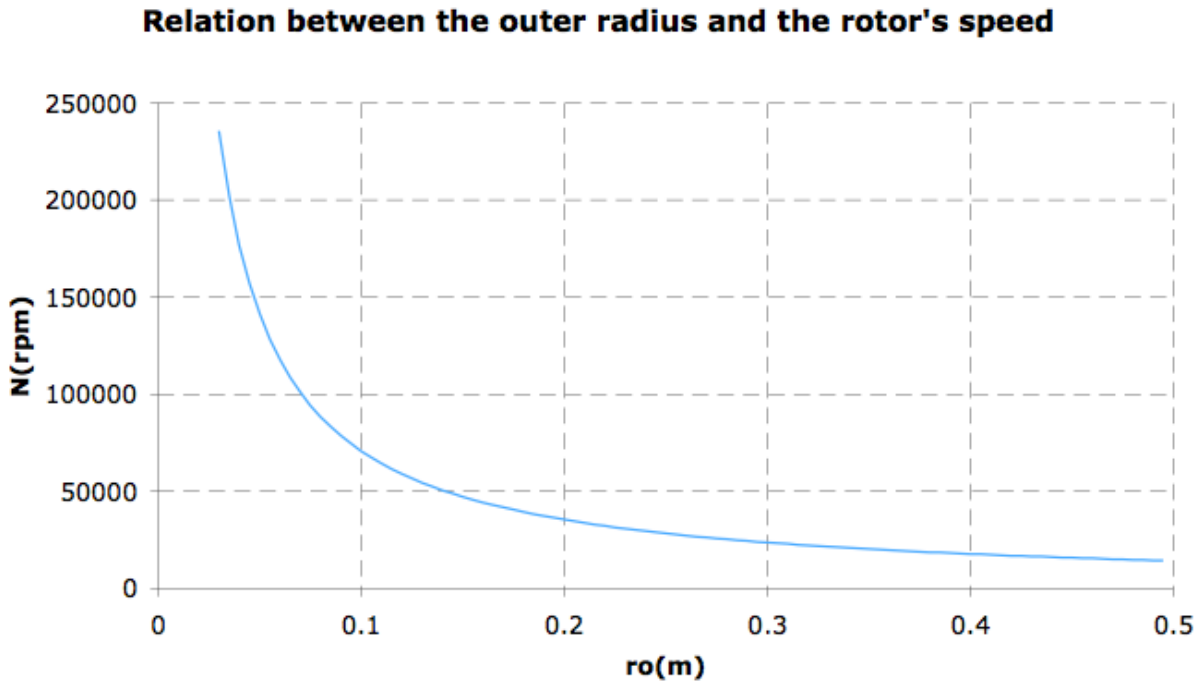

Figure 2.4. Relation between the outer radius and the rotor's speed, for carbon AS4C.

- *Using the achieved tangential stress approximation on the flywheel's fundamental equations:*

The finding of the stresses (equations (2.8) and (2.9)) is an important factor for the study of tensile stress.

The maximum of equation (2.8) is for $r = \sqrt[4]{r_o^2 \cdot r_i^2}$ and then it can be conclude that $\sigma_{r,\max} = \frac{3+v}{8} \cdot \rho \cdot \omega^2 \cdot \left(r_o - r_i\right)^2$.

Function (2.9), gets its maximum when r=r_i. So, the critical equation is given by (2.12):

$$\sigma_{t\max} = \frac{3+v}{8} \cdot \rho \cdot \omega^2 \cdot r_o^2 \cdot \left(2 + \left(1 - \frac{1+3 \cdot v}{3+v}\right) \cdot \left(\frac{r_i}{r_o}\right)^2\right) \tag{2.12}$$

Using the approximation $\frac{\sigma_t}{\rho \cdot \omega^2 \cdot r_o^2} \approx 1$, in equation (2.5), the energy limit (in [*MJ*]) can be achieved:

$$E_{\lim} = \frac{1}{4} \cdot \pi \cdot h \cdot \left(1 - \left(\frac{r_i}{r_o}\right)^4\right) \cdot r_o^2 \cdot \sigma_t \tag{2.13}$$

Taking into account the consideration above, the energy limit per total volume (in [MJ/m^3]) is given by the next equation (with $a = \frac{r_i}{r_o}$):

$$E_{\lim\_per\_volume} = \frac{1}{4} \cdot \left(1 - a^4\right) \cdot \sigma_t \tag{2.14}$$

The energy limit per total volume of rotating mass (in [MJ/m^3]) is represented by equation (2.15):

$$E_{\lim\_per\_volume\_mass} = \frac{1}{4} \cdot \frac{\left(1-a^4\right) \cdot \sigma_t}{1-a^2} = \frac{1}{4} \cdot \frac{\left(1-a^2\right) \cdot \left(1+a^2\right)}{1-a^2} \cdot \sigma_t = \frac{1}{4} \cdot \left(1+a^2\right) \cdot \sigma_t \tag{2.15}$$

Having now these two equations (represented on the next graphic), it is possible to find the ideal relation between the inner radius and the outer radius, $a = \frac{r_i}{r_o}$.

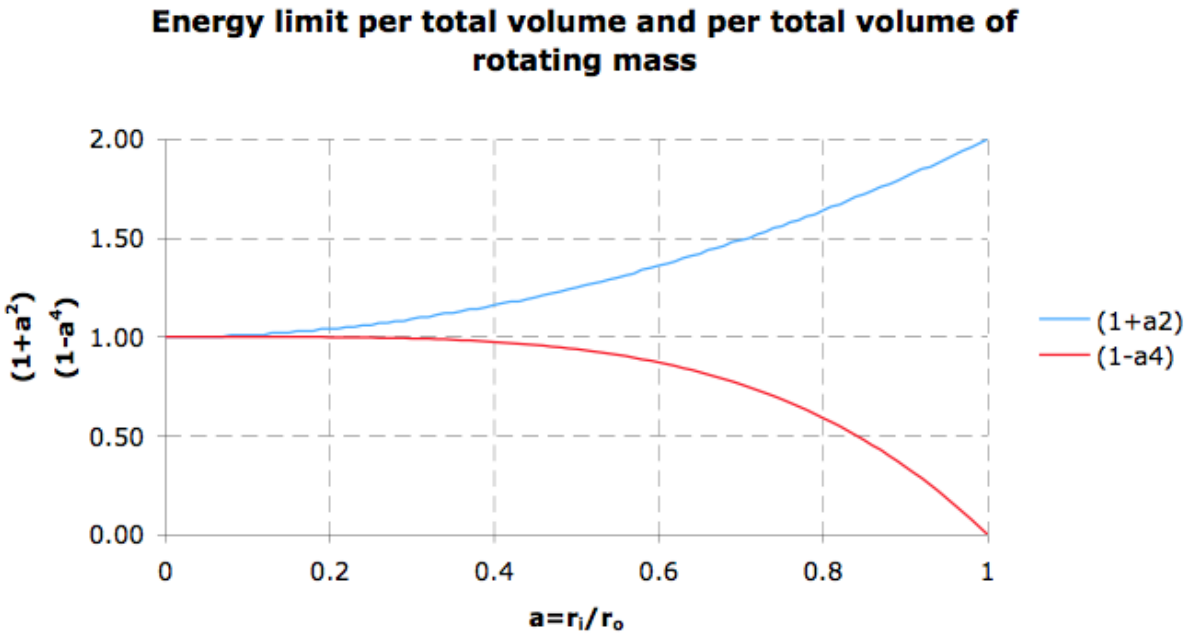

Figure 2.5. Representation of energy limit per total volume, in blue ($1+a^2$) and energy limit per total volume of rotating mass, in red ($1-a^4$).

It can be seen that the best relation between the inner radius and the outer radius is around 0.7; this value will be confirmed in the next calculations.

- *Calculation to find the best relation between the inner radius and the outer radius,* $a = \frac{r_i}{r_o}$*:*

To find the best relationship between r_i and r_0, it's very important to maximize the relationship between the wheel volume and its mass.

$$F = \alpha \cdot \left(1 - a^4\right) + \left(1 - \alpha\right) \cdot \left(1 + a^2\right)$$

With $\alpha = \frac{1}{2}$, as an example, the equation above results in:

$$2F = \left(1 - a^4\right) + \left(1 + a^2\right)$$

This equation will now be derived in order to obtain the maximum value of *a*:

$$\frac{dF}{da} = -4 \cdot a^3 + 2 \cdot a = 0 \Rightarrow a^2 = \frac{1}{2} \Rightarrow a = \frac{\sqrt{2}}{2}$$

It can be concluded that the best relation between the inner radius and the outer radius is $\frac{\sqrt{2}}{2}$.

2.2.3 Flywheel rotor's geometry and materials

- *Relation between the energy storage capability and the flywheel geometry:*

The speed is limited by the stress developed in the wheel, called tensile strength, σ.

A more general expression for the maximum energy density, valid for all flywheel shapes, is given by equations (2.16) and (2.17), which were obtained from [5].

$$e_v = K \cdot \sigma \tag{2.16}$$

$$e_m = \frac{K \cdot \sigma}{\rho} \tag{2.17}$$

Where e_v is the kinetic energy per unit volume and e_m per unit mass, K is the shape factor, σ is the maximum stress in the flywheel and ρ is the mass density. The shape factor K is a constant that represents the cross section geometries and its value is less than 1, as shown in table 2.1.

The adopted flywheel geometry was a hollow cylinder. This geometry was chosen due to its simpler manufacture and lower cost, when compared to other geometries.

Table 2.1. Shape factor K for different planar stress geometries. [26]

Fly wheel geometry	Cross section	Shape factor K
Disc		1.000
Modified constant stress disc		0.931
Conical disc		0.806
Flat unpierced disc		0.606
Thin firm		0.500
Shaped bar		0.500
Rim with web	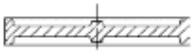	0.400
Single bar	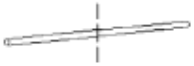	0.333
Flat pierced bar		0.305

Since the hollow cylinder is not represented in the table, the chosen value for its shape factor was the same as the thin firm (K=0.5), because it's the one that has a similar geometry.

- *Rotor materials:*

The materials that compose the flywheel's rotor will limit its rotational speed, due to the tensile strength developed. Lighter materials develop lower inertial loads at a given speed, therefore composite materials, with low density and high tensile strength, are excellent for storing kinetic energy.

Table 2.2 shows characteristics of several materials used on wheels. The analysis of the table confirms that the carbon composite materials are the ones that maximize the energy density.

Composite materials are a new generation of materials that are lighter and stronger than the conventional ones, like steel.

For the simulations carbon AS4C was chosen because it is the second best on tensile strength and on energy density and less than half the price of the first one.

Table 2.2. Characteristics for common rotor materials. [27]

Material	Density (kg/m^3)	Tensile strength (MPa)	Max energy density (for 1 kg)	Cost ($/kg)
Monolithic material 4340 Steel	7700	1520	0.19 MJ/kg = 0.05 kWh/kg	1
Composites				
E-glass	2000	100	0.05 MJ/kg = 0.014 kWh/kg	11.0
S2-glass	1920	1470	0.76 MJ/kg = 0.21 kWh/kg	24.6
Carbon T1000	1520	1950	1.28 MJ/kg = 0.35 kWh/kg	101.8
Carbon AS4C	1510	1650	1.1 MJ/kg = 0.30 kWh/kg	31.3

2.3 Flywheel rotor's dimensions, weight and material's cost

The relation that maximises energy with less material and speed will be now applied to design a wheel that can be used in a flywheel system application.

Some calculations have been made to the design of a flywheel rotor's dimensions, weight and material's cost (and are represented in Annex 2) starting with the 1st series of calculations, which was the most successful one, to the 4th series of calculations.

To calculate the rotor's weight, the density of ρ=1510Kg/m^3 was used, and to calculate the material's cost, the carbon price of 31,3$/Kg was used (values taken from table 2.2).

The series of results achieved in Annex 2 were compared to the weight and volume of each wheel, as table 2.3 shows.

Table 2.3. Rotor's dimensions, weight and material's price for different energy capacities.

E_{lim}	N (rpm)	r_o (m)	r_i (m)	h (m)	Occupied volume (m^3)	Material's volume (m^3)	Weight (Kg)	Material's cost ($)
2.5 kWh; 9MJ	33613	0.21	0.148	0.42	0.06	0.03	44	1385
2.5 kWh; 9MJ	42350	0.167	0.118	0.667	0.06	0.03	44	1385
1kWh; 3.6MJ	45620	0.155	0.109	0.31	0.02	0.01	18	558
25 kWh; 90MJ	15602	0.452	0.32	0.905	0.6	0.3	438	13706
0.44kWh; 1.58MJ	60000	0.118	0.083	0.235	0.01	0.005	8	245

By the analysis of table 2.3, the most interesting results are the 1st and 4th series of calculations (lines 1 and 2 of the table). It can be concluded that the energy depends on the gyrating volume and not directly on the rotor's radius and height. As it can be seen, both 1st series and 4th series have a wheel with the same energy capability storage, the same mass and the same price. It is also shown that in the 4th series it occupies more space and still needs to spin faster than in the 1st series.

Based on the results shown in table 2.3, a flywheel energy-storage system with 5 kWh capacity could be designed for the application on an electric vehicle, having two robust rotors of 2,5 kWh, each one, and the transformation between rotational kinetic energy and electrical energy would be performed with two permanent magnet motor/generator of 30 kW (40.23 hp) each.

It was chosen to use two rotors of 2,5 kWh instead of one rotor of 5 kWh, in order to fit the free area inside an automobile.

Using the 1st series of calculations, each rotor has a mass of 44 kg and uses a carbon-fiber composite rim (for the two rotors, the material's cost is around $3000), combined with a solid metallic hub, to create a rotor without critical resonances within the normal operating range.

2.4 An example for the use of the wheel

Based on the section 2.3 results, according to the wheel design and its energy capability, a wide range of applications for the wheel can be defined and imagined, one of them could be an electrical system that needs great power capability, as for instance, a flywheel energy system bus.

For this system, electrically, the motor/generator of each flywheel could be connected to the same dc bus through its own inverter and filter, as shown in figure 2.6.

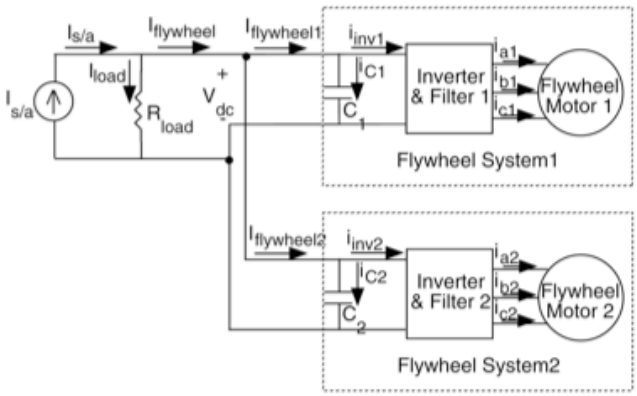

Figure 2.6. Electrical schematic of the two flywheels connection. [2]

In charge mode, the dc current $I_{flywheel}$ is positive and the speed of the flywheels is increasing. In discharge mode, the flywheels are decreasing in speed and providing power to the dc bus.

From figure 2.6 it can be concluded that this implementation maintains both flywheels with the same amount of energy.

An example of one of the flywheels used in the system above is shown in figure 2.7.

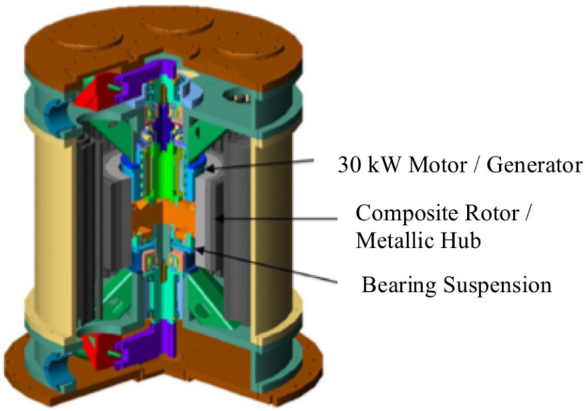

Figure 2.7. Cutaway view of a flywheel energy-storage system. [3]

The flywheel energy-storage system represented in figure 2.7 will have rotor of 2,5 kWh and a permanent magnet motor/generator of 30 kW (40.23 hp). The rotor will have a mass of 44 kg and the material's cost will be around $1400.

Chapter 3

Overview of Motors/Generators used in Flywheels

This chapter describes different electrical machines for possible application at a flywheel and presents a study of the work performed up to date. After this study, it was concluded that one of the most appropriate machines to use at the flywheel designed in Chapter 2 is a Permanent Magnet Synchronous Machine.

3.1 Introduction

Flywheels are complex constructions where energy is stored mechanically and transferred to and from the flywheel by an electrical machine.

The electrical machine should work as a motor to transfer electrical energy to the flywheel and as a generator to restore the energy stored into the flywheel. When acting as a motor, the electric energy supplied to the stator winding is converted into mechanical energy, increasing the speed of the flywheel. In generator mode, kinetic energy stored in the rotor is transformed into electrical energy.

The motor/generator part has a large upgrade potential and its design is continuously improving [5].

The next figure shows the basic layout of a flywheel energy storage system.

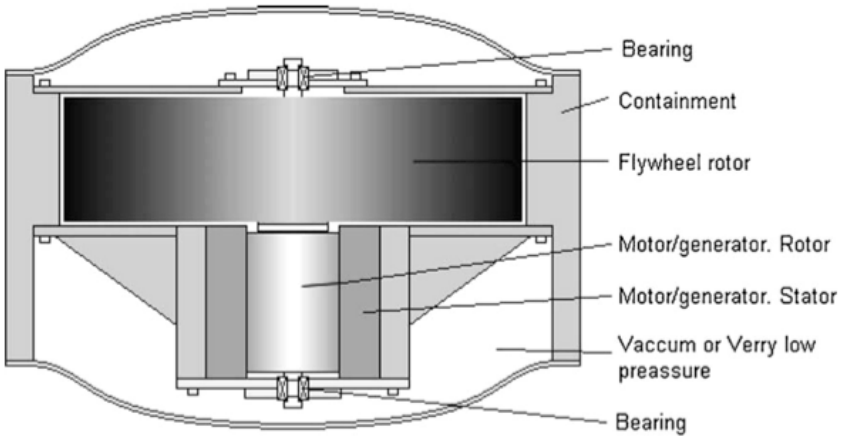

Figure 3.1. Basic layout of a flywheel energy storage system. [25]

In theory, it would be advantageous to build a generator that produces high voltage (considered in [5] as >10kV, for flywheels) and low current, which would result in high power supply and low power losses.

The fast rotation of flywheel rotors is suitable for direct generation of high voltage.

Next, there is an overview of flywheel technology, its applications and present development, at the work performed up to date [5]:

Peak power buffers – The flywheel could be used in an electric vehicle to eliminate peak currents that prolongs the battery life.

Wind-diesel generator with a flywheel energy storage system – The goal of this system was a unit where the regular wind oscillations were compensated by the flywheel, supplying active and reactive power to compensate both frequency and voltage of the network.

Flywheel for photovoltaic system – Despite the many benefits of using solar energy, its frequent unavailability makes it inappropriate for many applications. Consequently it is often necessary for photovoltaic (PV) systems to have an energy storage capability such that the excess output of the PV cells can be used at a time when solar energy is unavailable. As an example of this kind of application, in a photovoltaic equipped building situated in Hong Kong, the load supply time was prolonged from 9 a.m. - 3 p.m. to 8 a.m. - 6 p.m., by adding a flywheel.

Harmonics – The basic principle of flywheel harmonic compensators is similar to the active filter using an inverter. However the flywheel system has an energy storage capability additionally. In the active filters, compensation currents are estimated for reducing the harmonics by calculating harmonics of the load current. Then the estimated current is generated by an inverter. Different flywheel systems for compensating harmonics in low voltage were compared and analyzed. Up to the eleventh harmonic, a decrease of about 50% was accomplished.

Flywheel in distribution network – The flywheel can be used to maintain high quality electric power and guarantee a reliable power supply from the distribution network (it was able to keep the voltage in the distribution network within 98–102% and had the capability of supplying 10 kW of power for 15 min).

High power UPS system – For a high power system, 25 flywheels were connected

in parallel, with possible applications on energy supply for plasma experiments, accelerations of heavy masses (aircraft catapults on aircraft carriers, pre-acceleration of spacecraft) and large UPS systems. Similar permanent magnets flywheels have previously been tested in urban traffic buses and rail systems with a resulting energy save of up to 40%.

UPS system – As an example of this kind of application, four flywheel based dynamic UPS systems were connected to the distribution network; it resulted in a significant improvement in power quality. A transformer was required between the flywheel storage system and the medium voltage network.

Aerospace applications – A flywheel storage unit was intended to replace a battery storage unit onboard the International Space Station, a comparison between the flywheel and the NiH2 battery has shown that a flywheel system would be 35% lighter and 55% smaller in volume.

3.2 Types of electric machines for possible application in flywheels

Requirements for standardized electric power have made most flywheel systems use variable speed AC generators (because of the gradual speed reduction of the flywheel during discharge) and rectifiers to deliver DC electricity.

The two major types of machines used are the axial-flux and the radial-flux permanent magnet machines (AFPM and RFPM, respectively), as shown in figure 3.2.

The axial machines seem to have more advantages over the radial such as, a planar adjustable air gap and easy cooling arrangements, which is important when working under low-pressure conditions [5].

The radial flux machine is mostly used in small-scale high-speed machines, where the tensile strength of the permanent magnets demands placing close to the rotating axle.

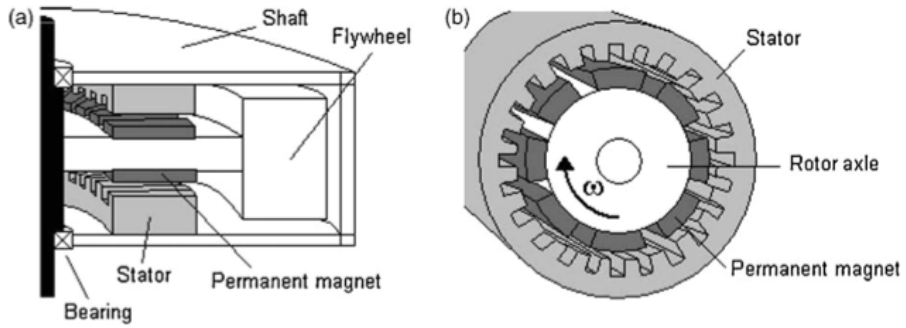

Figure 3.2. (a) AFPM machine arrangement and (b) RFPM machine arrangement. [5]

Another type of motor/generator is the internal-dipole, Halbach-type magnet array, where the permanent magnets array rotates with the flywheel and interacts with a set of stationary coils to produce torque.

The Halbach type motor can also be of multi-pole type.

A cross section of an internal dipole array with 8 segments, where M is the magnetization, is shown in figure 3.3, inside a single turn two-phase stator.

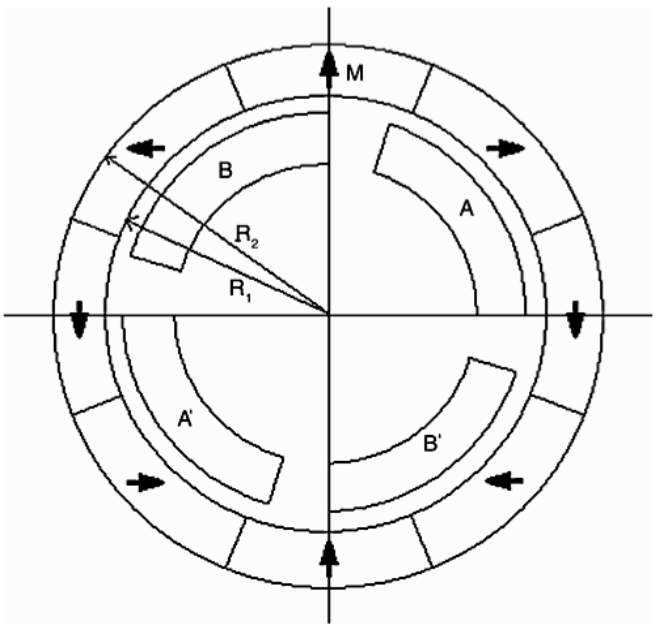

Figure 3.3. Cross section of internal dipole array for n=8. [5]

- *High voltage*

In spite of progresses in the flywheels technology, there's still one common problem,

the inability to directly produce high voltage (>36 kV) [5].

Some ‘high voltage’ flywheels have been constructed, however, the highest voltage attained so far was a 10-pole permanent magnet machine with a peak voltage of 10 kV, constructed in 2001 [5].

Apart from the permanent magnet motor/generator used in almost all flywheels there is also the possibility of using a synchronous reluctance motor/generator [5]. In 1996 a 60 kW flywheel, using this type of machine, was developed.

The next table shows the advantages and disadvantages of permanent magnet and induction machines, for this application.

Table 3.1. Advantages and disadvantages of permanent magnet and induction machines [5]

	Advantages	Disadvantages
High voltage permanent magnet machine	– High overload capability, due to low load angle and low stator current – Magnetic field is produced without excitation losses – Less complex rotor design, no need of electric wires in the rotor – Possible to achieve a higher overall efficiency	– Risk of demagnetization and a decreasing intrinsic coercivity with increasing temperature – Machines with iron in the stator experience electromagnetic mechanical losses at zero-torque – The low tensile strength of PM materials require structural support against centrifugal forces leaving constraints on the design of high-speed, high-power rotors

Permanent magnet machine	– Magnetic field is produced without excitation losses – Less complex rotor design, no need of electric wires in the rotor – Possible to achieve a higher overall efficiency	– Risk of demagnetization and a decreasing intrinsic coercivity with increasing temperature – Machines with iron in the stator experience electromagnetic mechanical losses at zero-torque – The low tensile strength of PM materials require structural support against centrifugal forces leaving constraints on the design of high-speed, high-power rotors
Induction machine	– No concern with demagnetization – No excitation field at zero torque, hence no electromagnetic mechanical losses – Can be constructed from high-strength low-cost materials	– RI^2, transformer and rectifying losses in the electromagnets during field excitation – Poor overload capability due to the high stator current

- *Number of poles*

The two pole motor/generators are the most common in high-speed machines, mainly to keep the frequency not very high and, consequently, the voltage amplitude too. [5]

3.3 State of the art of electrical machines used in flywheels

The next table resumes some motors/generators described in different articles, for the application at flywheels. This table was organized in order to identify, for each type of machine, the country of development, the year of development and the correspondent machine parameters.

Table 3.2. Some motors/generators described in different articles, for the application on flywheels

Country of development	Type of machine	Year of development	Machine parameters
USA [7]	Halbach-Array motor/generator	2001	*Rotor*: 1.5 Nm of torque; 28 000 rpm; 2kWh; *Machine*: 208V; 3 phase-Yconnected; 20.2 cm of diameter; 0.6 cm of thickness; 15.5 cm of height
USA [8]	Permanent magnet conventional motor/generator with toothless back iron	2002	
Japan [9]	Synchronous reluctance motor/generator	2000	*Machine*: 180W; 200V; 1.2A; 4 poles
Japan [10]	Permanent magnet synchronous motor/generator	2006	*Machine*: 4 pole pairs

China [11]	Surface permanent magnet synchronous motor/generator	2006	*Rotor*: 50 000 rpm; *Machine*: 1.2kW; 400V; 2.8A; 6 poles
NASA, USA [12]	Permanent magnet synchronous motor/generator	2004	*Rotor*: 320Wh; 60 000 rpm *Machine*: 1kW; 2 pole; 3 phase-Y connected; DC Bus voltage; 130V
Sweden [5]	Permanent magnet axial-flux motor/generator	2007	*Rotor*: 8 000 rpm; 5kWh; 30Kg; 1m of diameter *Machine*: 200kW; 3 phase; 1kV; 115.5A; 0.689m of outer diameter; 12 poles; Possible application at a bus, or for stabilizing the electric grid; NdFeB permanent magnets.
USA [13]	Permanent magnet synchronous motor/generator	1998	*Rotor*: 110 000 rpm; 11.9 kW/kg
Japan [14]	Permanent magnet motor/generator	2007	*Machine*: 3 phase; 4 poles; 1.5kW
Japan [15]	Permanent magnet axial-flux motor/generator	2003	*Rotor*: 3 000 rpm; *Machine*: 4.20kW; 153V; 15.9A; (17kW at 10 000rpm)

USA [16]	Synchronous Homopolar Motor	2002	*Rotor*: 50 000rpm – 100 000rpm; 36 Kg *Machine*: 30kW; 140Wh; 11.2 cm of diameter; 11.5 cm of length; 3.8 cm of height; 9.5 Kg

In conclusion, the most used is the Permanent Magnet Synchronous Machine, including in the most recent works. This machine was chosen due to its efficiency, smaller size and easier control, when compared to direct current machines or induction machines.

Chapter 4

Preliminary Design of a Permanent Magnet Synchronous Machine

This chapter presents the design principles of a Permanent Magnet Synchronous Machine for application at the flywheel designed in Chapter 2.

The factors influencing the design are costs, material limitations, standard specifications and special application factors. The major issues in designing the machine can be divided into 5 areas: electrical, magnetic, insulation, thermal and mechanical.

The stress forces at the machine's rotor were studied in order to guarantee that the materials used on the rotating mass have the strength to hold the stresses.

4.1 Introduction

On Chapter 3 it was concluded that the Permanent Magnet Synchronous Machine is, actually, one of the preferable choices for the motor/generator in flywheels.

In this chapter a preliminary design of this machine will be performed, which can lead to future and more extensive work.

The calculation for this design principles and analysis were made, considering a 30kW, 2 pole, 1000V, 15000 rpm and $\eta = 95\%$ machine, which was concluded, in the previous chapters, as being a good machine for the desired application.

Factors that influence the machine design remarkably are as follows [19]:

Costs: Costs in most cases are the overriding consideration in machine design. Global costs are a fundamental issue, when it is necessary to choose between repairing an old motor and replacing it with a new one (with higher efficiency and corresponding initial costs).

Material limitations: The costs of the materials are commensurate with performance. Progress in magnetic and insulation materials has been continuous. Such new improved materials drastically affect machines design (geometry), performance (efficiency), and costs. Flux density, B, losses in magnetic materials, current density in conductors and dielectric rigidity E and thermal conductivity of insulation materials are key factors in machine design.

Standard specifications: Parameters specified in national (or international) standards (NEMA, IEEE, IEC, EU, etc.) to facilitate globalization in using machines in various applications, limit the designer's options, but provide solutions that are widely accepted and economically sound.

Special factors: In special applications, special specifications become the main concern. For example, aircraft applications need minimum weight and maximum reliability and transportation applications require easy maintenance, high reliability and good efficiency.

The major issues in designing a machine may be divided into 5 areas: electrical, dielectrical, magnetic, thermal and mechanical [19].

Electrical design: To supply the machine, the supply voltage, frequency, and number of phases are specified. From this data and the minimum power factor and the target efficiency, the phase connection (star or delta), winding type, number of poles, slot numbers and winding factors are calculated. Current densities are imposed.

Magnetic design: Based on output coefficients, power, speed, number of poles, type of cooling, and the rotor diameter is calculated. Then, based on a specific current loading and airgap flux density, the stack length, L, is determined. Sizing the stator and rotor core may be done in different ways, based on various criteria.

Insulation design: Insulation material and its thickness (slot/core insulation and conductor insulation) depends on machine voltage insulation class and the environment in which the motor operates.

Thermal design: Depending on application or power level, various types of cooling are used. Calculating the loss and temperature distribution and the cooling system, represents the thermal design.

Mechanical design: Mechanical design refers to critical rotating speed, noise, and vibration modes, mechanical stress in the shaft, and its deformation displacement, bearings design, inertia calculation, and forces on the winding end coils during most severe current transients.

4.2 Output equation and main dimensions

Considering a full-pitch, single-turn coil in a magnetic field that is sinusoidally distributed in space and is sinusoidally varying in time [17].

The rms value of the voltage induced in the coil is:

$$E = \frac{2 \cdot \pi}{\sqrt{2} \cdot f \cdot \phi_p} = 4.44 \cdot f \cdot \phi_p \tag{4.1}$$

The rms voltage induced in the entire phase winding, with the number of turns equal to N_{ph} and a winding factor of K_w, is then:

$$E_{ph} = 4.44 \cdot f \cdot K_w \cdot N_{ph} \cdot \phi_p \tag{4.2}$$

$$E_{ph} = 4.44 \cdot \left(\frac{p \cdot N}{120} \right) \cdot K_w \cdot N_{ph} \cdot \left(B_{gav} \cdot \pi \cdot \frac{D \cdot L}{p} \right) \tag{4.3}$$

Now, if A is the specific electric loading, given at [17], then:

$$A = \frac{2 \cdot \left(3 \cdot N_{ph} \right)}{\pi \cdot D} \cdot I_{ph} \tag{4.4}$$

The apparent power of the machine can be written as:

$$S_{kVA} = 3 \cdot I_{ph} \cdot E_{ph} \cdot 10^{-3} \tag{4.5}$$

$$S_{kVA} = \frac{4.44 \cdot \pi^2}{240} \cdot K_w \cdot A \cdot B_{gav} \cdot D^2 \cdot L \cdot N \cdot 10^{-3} \tag{4.6}$$

If η is the efficiency and cosφ is the power factor of the machine, then:

$$\frac{P_{kW}}{\eta \cdot \cos\varphi} = \frac{4.44 \cdot \pi^2}{240} \cdot K_w \cdot A \cdot B_{gav} \cdot D^2 \cdot L \cdot N \cdot 10^{-3} \tag{4.7}$$

$$P_{kW} = \frac{4.44 \cdot \pi^2}{240} \cdot K_w \cdot A \cdot B_{gav} \cdot D^2 \cdot L \cdot N \cdot 10^{-3} \cdot \cos\varphi \cdot \eta \tag{4.8}$$

The next equation relates machine dimensions with its power rating, and is known as the output equation:

$$D^2 \cdot L \cdot N = \frac{5480}{A \cdot B_{gav} \cdot K_w \cdot \cos\varphi \cdot \eta} \cdot P_{kW} \tag{4.9}$$

$$D^2 \cdot L = \frac{5480}{A \cdot B_{gav} \cdot K_w \cdot \cos\varphi \cdot \eta \cdot N} \cdot P_{kW} \tag{4.10}$$

From equation (4.9), some aspects of machine design can be concluded:

- High-speed machines are smaller in size than low-speed machines;
- Using higher values of specific electric and magnetic loadings, machine size can be reduced. However, it results in temperature rise and magnetic saturation, thus creating an effective lower limit on size.

- *Specific Electric Loading, A* [17]:

The maximum value of *A* is limited by permissible *J*, which therefore is limited by the effectiveness of the cooling system.

For air-cooled motors, the nominal value of *A* is 15-35 ampere-conductors per millimetre (15000-35000 ampere-conductors per metre).

For the machine design, in our example, it will be used *A*=20000 ampere-conductors per metre, as an indicative value.

- *Specific Magnetic Loading, B_{gav}:*

The permissible value of B_{gav} is essentially limited by the maximum value of flux density in the teeth. The B-H curve describes the cycling of a magnet in a closed circuit as it is brought to saturation, demagnetized, saturated in the opposite direction, and then demagnetized again under the influence of an external magnetic field.

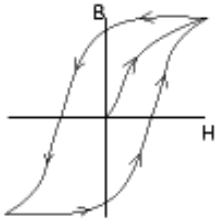

Figure 4.1. B-H curve or hysteresis loop.

The three most important characteristics of the B-H curve are represented in the next figure. These are the points at which it intersects the B and H axes (respectively B_r, the residual induction and H_c, the coercive force) and the point at which the product of B and H are at a maximum (BH_{max}, the maximum energy product).

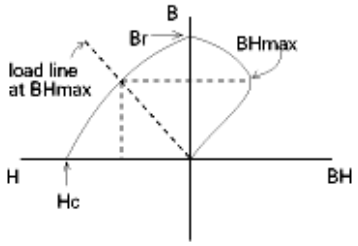

Figure 4.2. Second quadrant of the B-H curve, "Demagnetization Curve".

BH_{max} represents the point at which the product of B and H, and the energy density of the magnetic field into the air gap surrounding the magnet, is at a maximum.

B_{gav} is usually 0.35-0.60 Wb/m^2 for 60 Hz machines, so that the maximum tooth flux density can be limited to a high of 1.6 Wb/m^2.

For the machine design example, B_{gav}=0.6Wb/m^2 will be used, obtained approximately from half of the B_r (B_r=1.2Wb/m^2).

- *Winding Factor, K_w* [18]:

The next table represents the winding factors, between the 1st and the 15th harmonics, for different values of slots per pole per phase, q:

Table 4.1. Winding factors for different values of slots per pole per phase. [18]

	q=2	q=3	q=∞
K_{w1}	0.966	0.960	0.955
K_{w3}	0.707	0.667	0.636
K_{w5}	0.259	0.217	0.191
K_{w7}	-0.259	-0.177	-0.136
K_{w9}	-0.707	-0.333	-0.212
K_{w11}	-0.966	-0.177	-0.087
K_{w13}	-0.966	0.217	0.075
K_{w15}	-0.707	0.667	0.127

Since the 3rd harmonic doesn't have influence and harmonics above the 3rd can be neglected, the 1st harmonic is the most important.

For the machine design example, a winding factor of K_w=0.966 will be used, which corresponds to a 2 slots per pole per phase machine.

- *Aspect Ratio, $\frac{L}{\tau}$*:

The ratio of length (L) to pole pitch (τ) is called the aspect ratio. This ratio is chosen on the basis of several factors such as peripheral velocity (υ=2.f.τ), the end winding leakage flux, and other economic considerations such as cost of assembling the machine.

The optimal values range for the aspect ratio are situated in an interval, which limits are highly dependent on the machine design specifications and applications. Generally, high-speed machines are longer so that the peripheral velocity can be limited to acceptable levels.

This interval could have different limit values, according to the desired application in each reference of the bibliography. For example, according to [17], the ratio $\frac{L}{\tau}$ is usually between 1.00 and 4.00, (with the lower range applicable to lower speeds) and according to [19], the ratio $\frac{L}{\tau}$ is usually between 0.60 and 3.00.

For the machine design example, an aspect ratio between 1.00 and 4.00 will be used.

- *Cooling of the machine*:

An accurate estimation of the thermal behavior of an electrical machine is important considering the fact that safe operating conditions and overloading capabilities are dependent on the temperature rise.

The axial machines have easier cooling arrangements than the radial ones, which is important when working under low-pressure conditions, as happens on vacuum. The increase in thermal load due to the low air-pressure around the motor/generator needs to be compensated by a cooling system. [5]

The way to deal with losses in an electrical machine is to cool off the excessive heat. The equipment needed for cooling and ventilation is therefore essential but, in a normal machine, also very expensive. Nowadays air, water or hydrogen can be used for cooling the rotor and the stator. Table 4.2 summarizes the most common cooling methods. [33]

Table 4.2. Different ways of cooling the machine. [33]

Traditional methods					Methods used in high voltage		
Type of cooling	Air	Hydrogen	Water	Hydrogen-water	Air	Water-air	Water
Meaning	Stator and rotor air-cooled	Stator hydrogen-cooled, rotor hydrogen or air-cooled	Stator air-cooled, rotor water-cooled	Stator hydrogen-cooled, rotor wa-ter- cooled	Stator and rotor air-cooled	Stator water - cooled, rotor air-cooled	Stator and rotor water-cooled

Low air pressure naturally decreases the heat transfer rate from the rotor to the stator, which results in a rapid rise of the magnet and rotor temperature in a very short time.

There is no trivial way to remove the heat generated in the magnets and thus, the estimation of the rotor eddy-current losses is particularly important. Especially in the case of vacuuming where the rotor to frame and rotor to stator convection resistances are relatively large, becoming the rotor heat removal a major problem. Excessive heat may result in the demagnetization of the magnets and rotor destruction. [35]

In the absence of airflow on vacuum, a water-cooling system could be used to cool our motor/generator, which seems to be a good choice due to the high efficiency of this system.

- *Derating* [19]:

Derating is required when the machine is supplied from a power grid that has a notable voltage harmonic content due to increasing use of PWM static converters. The time harmonic content of machine input voltages is the cause of additional winding and core losses. Such additional losses of rated power (and speed) would mean higher than rated temperature rise of windings and frame. To maintain the rated design temperature rise, the machine rating has to be reduced.

NEMA 30.01.2 suggests the derating of the machine as a function of harmonic voltage factor (HVF), as the next figure represents.

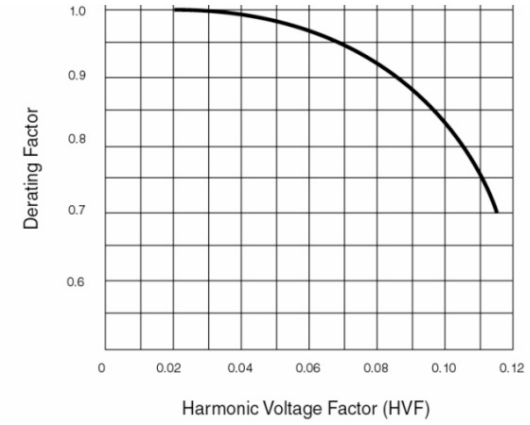

Figure 4.3. Derating for harmonic content of standard machines operating on sinewave voltage with harmonic content. [19]

In the figure, the derating factor represents the value that tells how much to reduce the power rating, due to harmonic distortion of the voltage signal (harmonic voltage factor).

The HVF can be calculated by analysing the voltage waveform, identifying the fundamental frequency, all harmonics present and their percent weight. It is defined as: $HVF = \sqrt{\sum_{n=5}^{n=\infty} \frac{V_n^2}{n}}$, where V_n is the RMS voltage at the nth harmonic as a percentage of the fundamental and n is the order of odd harmonic, excluding triple-n harmonics.

Reducing the HVF via power filters (active or passive) becomes a priority as the variable speed drives extension becomes more and more important.

Derating is not yet standardized, but it should be more important when power increases as the switching frequency decreases. A value of 10% derating for such a situation is now common practice [19]. The reduction factor is 5 to 10% depending on the PWM strategy in the converter.

If line voltage unbalance exists, the machine may be damaged and should be derated in accordance with the next figure, from NEMA Standard MG-20.55, in order to reduce the possibility of such damage. Derating factors, for several values of line voltage unbalance, are given below.

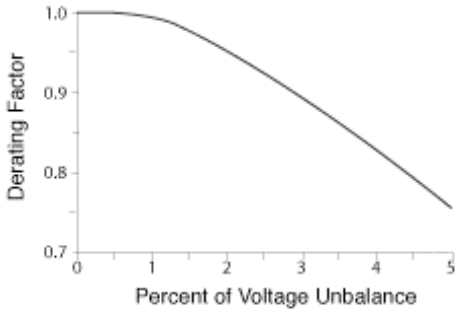

Voltage Unbalance	Approximate Derating
1%	None
2%	95%
3%	88%
4%	82%
5%	75%

Figure 4.4. Derating due to voltage unbalance. [19]

In the figure, the voltage unbalance represents the ratio (in per cent) between the rms values of the negative sequence component and the positive sequence component of the voltage, in a three-phase system.

This ratio may be approximated as:

$$\text{Voltage Unbalance (\%)} = \frac{\text{Maximum deviation from the average of the 3-phase voltages}}{\text{Average of the 3-phase voltages}} \times 100$$

It is further assumed that the machine is used without derating, to accommodate a high power factor control algorithm.

4.3 D_{in} and L calculation

The main dimensions D_{in} and L can be determined, using the output equation (4.10), for a given power rating of the machine.

The following parameters were used for the calculations in an illustrating example:

$P_{kW} = 30kW$ (This value was fixed)

$p = 2$ (This value was fixed)

$N = \frac{N_{\max}}{2} = \frac{33613}{2} = 16806.5rpm \approx 15000rpm$ (N_{max} obtained from Chapter 2)

$f = \frac{p \cdot N}{120} = \frac{2 \cdot 15000}{120} = 250Hz$

$B_{gav} = 0.6Wb/m^2$ (In order to obtain a working point near the BH_{max})

$K_w = 0.966$

$A = 20000ampere - conductors/m$

$\cos\varphi = 1$ (This value is a characteristic of the synchronous machine)

$\eta = 95\%$ (Common efficiency for a machine of this type)

Table 4.3 presents three different results for D_{in} and L (which series of calculations are explained in Annex 3) being the best result highlighted.

Table 4.3. Machine dimensions D_{in} and L.

Aspect Ratio, $\frac{L}{\tau}$	D_{in} (m)	L (m)	Calculations number
1.00	0.1082	0.0850	1st
4.00	0.0682	0.2142	2nd
N.A.	0.0499	0.4	3rd

Considering the available space inside the flywheel's rotor (a cylindrical hollow of 0.42 m height and 0.2 m radius), the best hypothesis seems to be the second one, due to the best use of L comparing to D, since is better to have a higher cylinder than a wider one. This conclusion was expected, because its calculation uses the aspect ratio applied to high-speed machines.

In the 3rd series of calculations, the aspect ratio is not available, because L was fixed in 0.4m (near the maximum height), then the $\frac{L}{\tau}$ wasn't needed.

4.4 D_{out} calculation

In this section, D_{out} represents the outer diameter of the stator bore and will be calculated, according to the obtained D_{in} (D_{in}=0.0682m).

The figure 4.5 represents the comparison of diameter ratio D_{in}/D_{out} without and with constraints on the surface current density, in order of the number of poles.

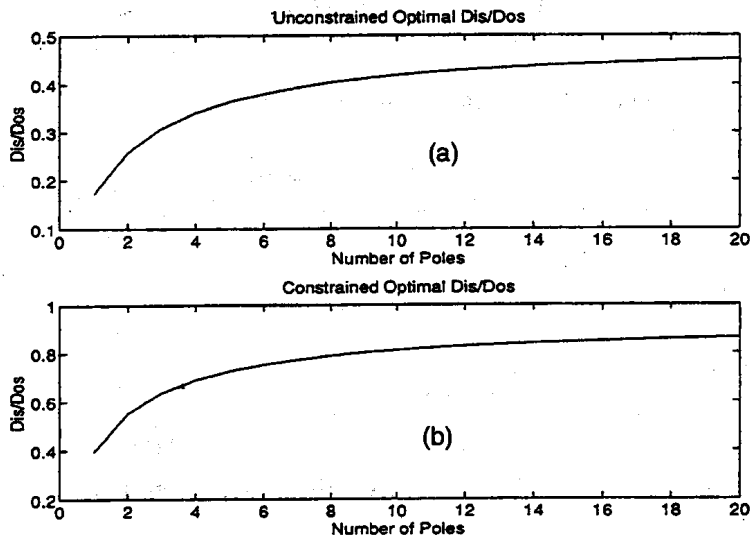

Figure 4.5. Comparison of diameter ratio D_{in}/D_{out} (a) without and (b) with constraints on the surface current density. [34]

Observing the figure 4.5, it is possible to conclude that, for a 2 pole machine:

Without constraints: $\frac{D_{in}}{D_{out}} = 0.25 \Rightarrow D_{out} = 0.2728m$

With constraints: $\frac{D_{in}}{D_{out}} = 0.55 \Rightarrow D_{out} = 0.124m$

Then, the maximum diameter of the machine will be of 0.2728 m.

4.5 Design equation of stator winding

The design of the stator winding follows the next steps [17]. This design is intended to calculate the conductors in series per phase, the number of stator slots, the slot pitch and the slot and tooth dimensions, those calculations will use the flux per pole:

- The flux per pole, $\phi_p = B_{gav} \cdot \frac{\pi \cdot D \cdot L}{p}$;
- Conductors in series per phase: $conductors/phase = N_{ph} \cdot 2 = \frac{E_{ph}}{2.22 \cdot f \cdot K_w \cdot \phi_p}$, obtained from equation (4.2), and the winding factor K_w = distribution factor × pitch factor. In the next calculation, a winding factor of K_w=0.966 will be used;
- For a machine with small number of poles, an integer number of slots per pole per phase (2, 3, 4, etc.) can be selected in order that the slot pitch ($\lambda = \frac{\pi \cdot D}{q}$) isn't too small. In the next calculation, a number of stator slots of $q = 2 pslots/pole/phase$ will be used;
- Calculate slot pitch, $\lambda = \frac{\pi \cdot D}{q}$;
- Obtain slot and tooth dimensions by having the ratio of tooth deep/tooth width <7, to avoid noise;
- Lay out a double-layer winding, $s = t = \frac{\lambda}{2}$.

4.6 Design calculation of stator winding

Following the previous steps, from 4.5, it was possible to achieve the results for the design of the stator winding.

The following parameters were used for the calculations:

$B_{gav} = 0.6 Wb/m^2$

$p = 2$

With $L = 0.2142m$ and $D = 0.0682m$ (which corresponds to the 2nd hypothesis of the D and L calculation)

$E_{ph} = 1000V$

$f = 250Hz$

$K_w = 0.966$

- The flux per pole: $\phi_p = B_{gav} \cdot \frac{\pi \cdot D \cdot L}{p} = 0.0138Wb$

- Conductors in series per phase:

$$conductors/phase = \frac{E_{ph}}{2.22 \cdot f \cdot K_w \cdot \phi_p} = 135.4737$$

Selecting an even number: $conductors/phase = 136$

$$N_{ph} = \frac{conductors/phase}{2} = 68$$

- Number of stator slots: $q = 2 pslots/pole/phase = 2 \cdot 2 \cdot 3 = 12 slots$

$$conductors/slot = \frac{conductors/phase}{\frac{q}{3}} = 34$$

- Slot pitch: $\lambda = \frac{\pi \cdot D}{q} = 0.0179m$

- Ratio of tooth deep/tooth width: $\frac{s}{t} = 1$

- Slot and tooth dimensions $s = t = \frac{\lambda}{2} = 0.0089m = 8.9mm$

4.7 Machine rotor stress forces

As it was seen in Chapter 2, materials like iron and another classic materials don't have the strength to hold high rotation speeds.

The synchronous machine was designed for 15000 rpm, and then, the materials used on the rotating mass, which supports the machine, must have the strength to hold the stresses.

The best option could be to choose the same material that was chosen for the flywheel's rotor (a carbon composite material, the carbon AS4C), which has a high resistance to twist forces.

4.8 Conclusions

In this chapter it was reported on and analyzed a previous study for the design principles of the Permanent Magnet Synchronous Machine that will be used on the flywheel.

The calculations considered a $P_{kW} = 30kW$, $p = 2pole$, $\eta = 95\%$, $E_{ph} = 1000V$ and $N = 15000rpm$ machine.

The main parameters of the proposed electrical machine are:

D	L	*conductors/phase*	q	*conductors/slot*	λ
0.0682m	0.2142m	136	12*slots*	34	0.0179m

It was possible to obtain a good previous design, which could be used in future, and more extensive work.

Chapter 5

Synchronous Machine Sensorless Control

This chapter provides a description of the most appropriate sensorless control methods for application to the Permanent Magnet Synchronous Machine designed in the previous chapter.

A sensorless control is desirable in order to reduce total hardware complexity, size, cost and maintenance requirements.

After the control principles and methods were studied, the Direct Flux and Torque Control was chosen for the desired application, as being one of the most efficient control systems.

5.1 Introduction

The permanent magnet synchronous machine (PMSM) was chosen for this work due to its efficiency, smaller size, and easier control as compared to direct current machine or induction machine.

The torque control of this machine requires knowledge of the rotor position to perform an effective control. Furthermore, for speed control (which is very important for performance improvement of the mechanical system), the speed signal is also required.

Vector control schemes for PMSM's require position sensors, like encoders or resolvers, in order to synchronize the phase excitation pulses to the rotor position.

For the successful industrial installation of the system, some considerations have to be taken into account, such as, the need to reduce total hardware complexity, size, cost and maintenance requirements and the need to increase drive's reliability and noise immunity.

For this propose it is desirable to eliminate these mechanical sensors in vector-controlled drives (which will be discussed in sections 5.4 and 5.5).

5.2 General considerations of electrical machines

For electric machines fed through power electronic converters, the term *base speed* ω_b, will be used, which represents the point where the flux will begin to decrease. The *maximum speed* ω_{max}, represents the speed limit of the machine. This limitation can be imposed by several electromagnetic or technological constraints.

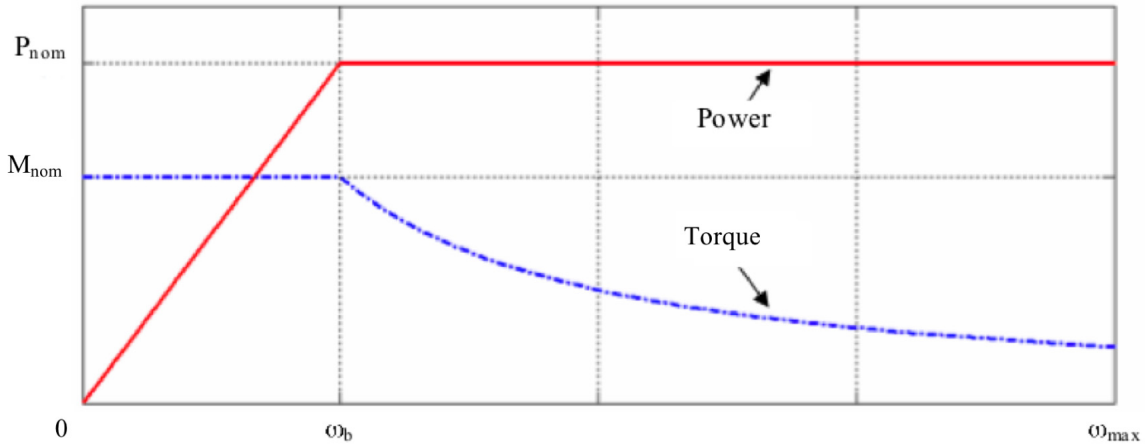

Figure 5.1. Power and Torque waveforms of an electrical machine. [32]

The figure 5.1 shows the waveforms of power and torque for an electrical machine. There can be distinguished two different zones [32]:

- Function below ω_b. In this zone, the nominal torque of the machine is available, but the maximum power varies directly with the speed, but below the nominal power.
- Function below ω_{max}. In this zone, the torque decreases in order to limit the power of the machine to its nominal value. So, the nominal power of the machine is available, whatever the speed is.

For the designed synchronous machine, the working zone will be in the interval below ω_b. Due to this fact, ω_b has to be dimensioned to a very high value, at least 15000 rpm (which is the maximum speed of the machine).

This is not according to the theory of electric machinery that says the better working zone is in the interval between ω_b and ω_{max}.

The figure 5.2 represents a simple schematic explanation of the system application in this work. It shows the Synchronous Machine working as a motor and as a generator, where the desired system is the flywheel.

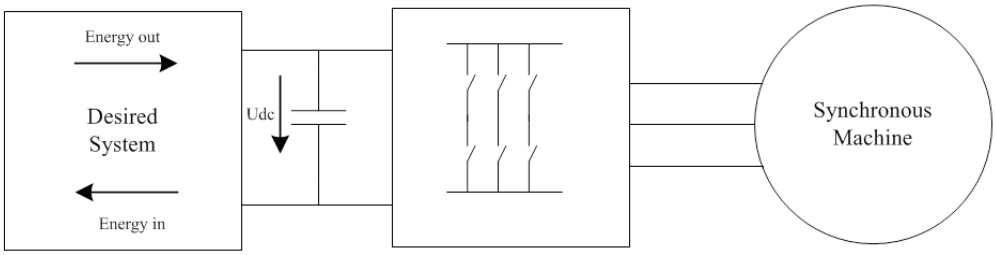

Figure 5.2. Schematic explanation of the desired system in this work.

The figure 5.2 can be divided in the next two different working schemes.

- *Control scheme of the Synchronous Machine working as a motor:*

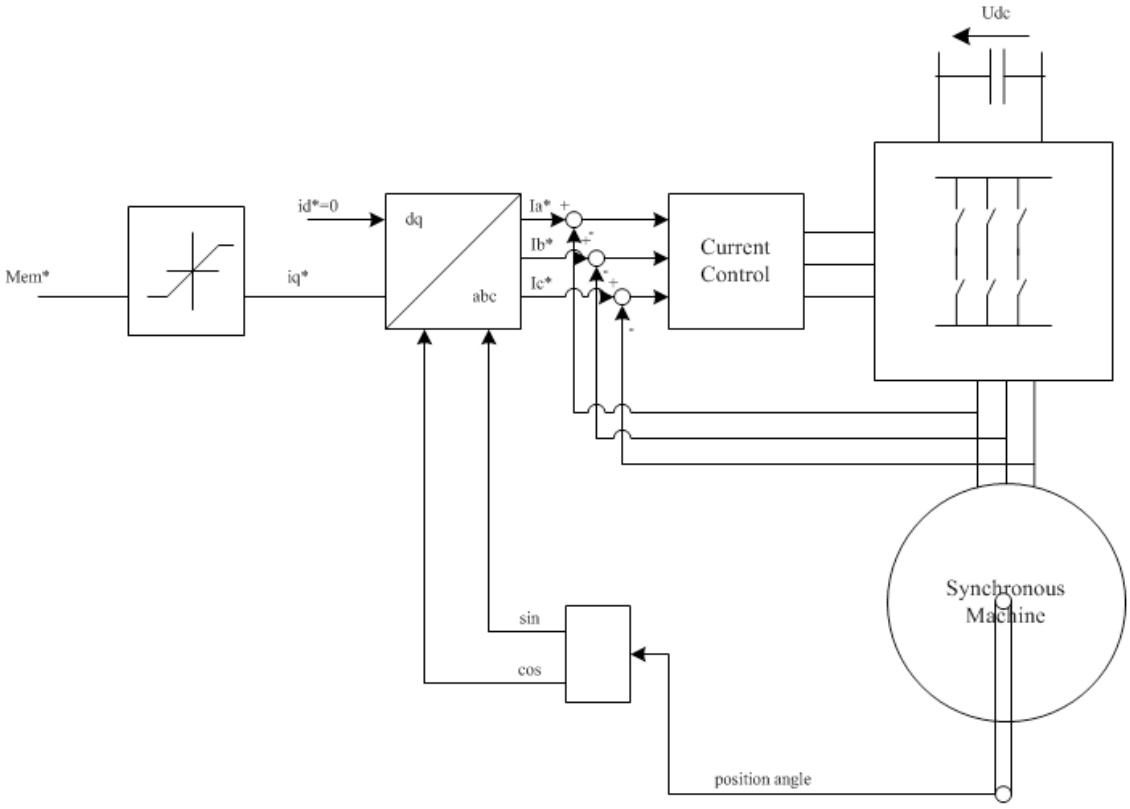

Figure 5.3. Control scheme of the machine working as a motor.

The figure 5.3 shows the overall control strategy proposed for controlling the torque of a synchronous motor.

By means of an absolute encoder or resolver, the sine and cosine of the angular position of the rotor were obtained.

The three reference currents I_a^*, I_b^* and I_c^* (where superscript ‘‘*’’ denotes the reference value) were obtained by the DQ/abc block, which represents the Park’s Transformation, using the reference currents, i_d^* and i_q^* and the position angle of the rotor.

- *Control scheme of the Synchronous Machine working as a generator:*

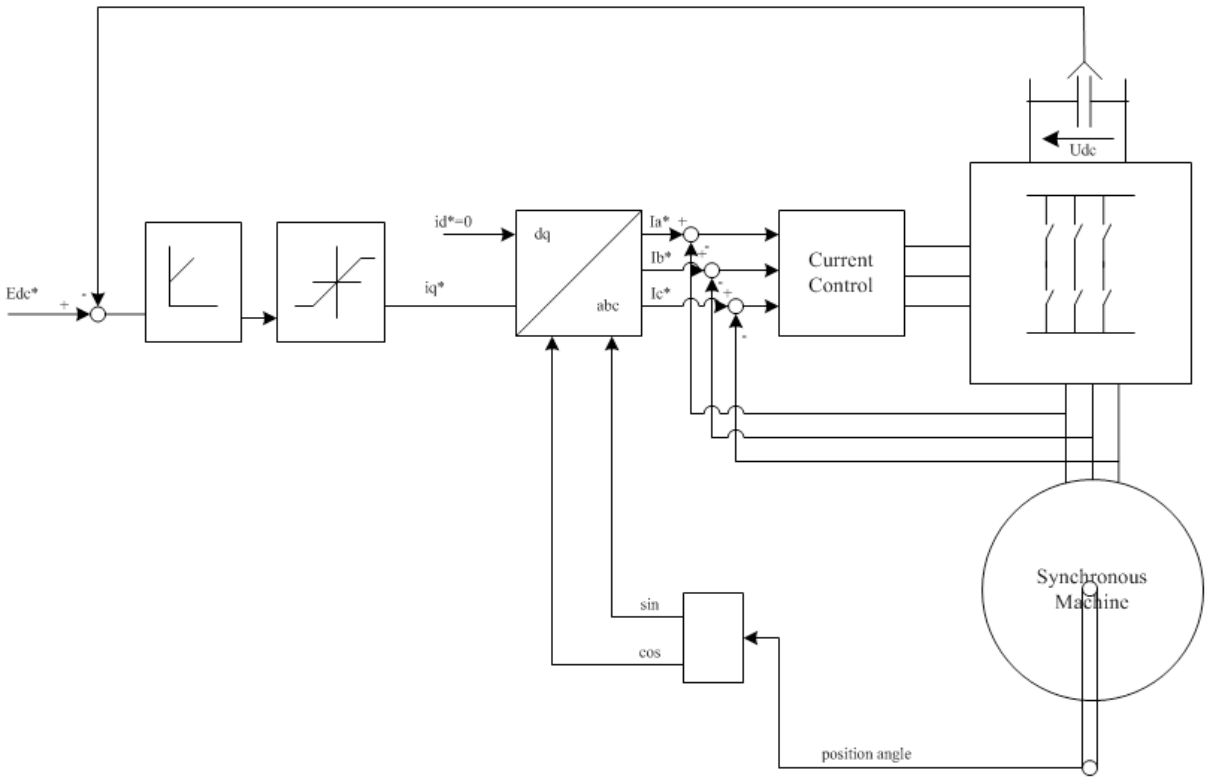

Figure 5.4. Control scheme of the machine working as a generator.

The figure 5.4 shows the overall control strategy proposed for controlling the dc voltage of the inverter that is connected to the synchronous generator.

The value of U_{dc} is a constant and will be acquired by an estimator, in order to compare it with its reference value. The obtained error will be an input of the PI controller.

By means of an absolute encoder or resolver, the sine and cosine of the angular position of the rotor were obtained.

5.3 Permanent Magnet Synchronous Machine classic control

Many methods have been presented in literature [20, 21] for detecting the rotor positions for different classes of PMSM, without mechanical sensors. Most of them have been developed for the IPMSM (interior permanent magnet synchronous machine) because the inductance variation in the direct- and quadrature-axis can be monitored easily in order to detect the rotor position.

These position sensorless control schemes have a fine speed and position control performance without a position sensor.

For the SPMSM (Surface Permanent Magnet Synchronous Machine), which is the chosen machine for this work, it is difficult to control the motor speed accurately when the angular rotor speed is very low or becomes zero.

However, in this application, the system is only needed for high speeds. The starting operation near zero speed can be done slowly until the sensorless position and speed become available.

The problem with the surface mounted rotor is the equal inductances along direct- and quadrature-axis, making the detection of rotor speed difficult in standstill and at low speed operation.

In addition, the SPMSM has more advantages than the IPMSM such as lower cost and simpler mechanical structure in industry applications [11]. As result, the research for sensorless control of the SPMSM is very significant.

- *Control system of a Permanent Magnet Synchronous Machine supplied by a current-controlled PWM voltage source inverter, using mechanical sensors:*

The figure 5.5 shows the scheme of a Permanent Magnet Synchronous Machine supplied by a current-controlled PWM voltage source inverter, and the current controllers are hysteresis controllers.

The figure 5.5 represents a basic scheme using position and speed mechanical sensors.

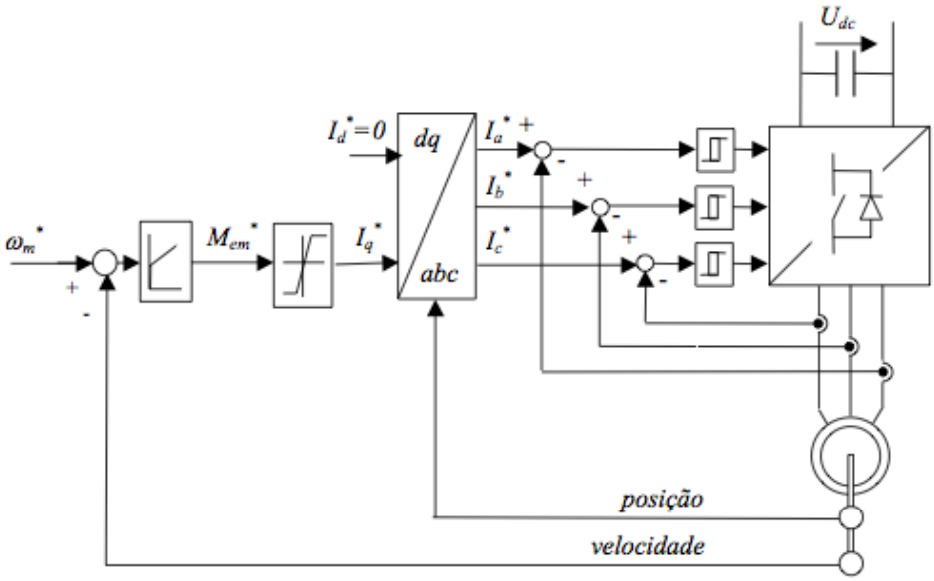

Figure 5.5. Control scheme, using mechanical sensors, of the Permanent Magnet Synchronous Machine supplied by a current-controlled voltage-source inverter. [20]

With superficial magnets (considering the approximation: $L_{sD} = L_{sQ} = L_s$), the voltage, stator flux linkage and electromagnetic torque equations expressed in the rotor flux reference frame (d–q coordinates) are:

$$u_{sD} = R_s \cdot i_{sD} + \frac{d\psi_{sD}}{dt} - \omega \cdot \psi_{sQ} \tag{5.1}$$

$$u_{sQ} = R_s \cdot i_{sQ} + \frac{d\psi_{sQ}}{dt} + \omega \cdot \psi_{sD} \tag{5.2}$$

$$\psi_{sD} = \psi_{sf} + L_{sD} \cdot i_{sD} \tag{5.3}$$

$$\psi_{sQ} = L_{sQ} \cdot i_{sQ} \tag{5.4}$$

$$M_{em} = p \cdot \left(\psi_{sD} \cdot i_{sQ} - \psi_{sQ} \cdot i_{sD} \right) \tag{5.5}$$

Where R_s is the stator winding resistance, p is the number of poles, ω is the angular frequency; ψ_{sD}, ψ_{sQ} are the d–q components of the stator flux linkage; ψ_{sf} is the rotor flux linkage generated by the permanent magnets; i_{sD}, i_{sQ} are the d–q components of the stator winding current; u_{sD}, u_{sQ} are the d–q components of the stator winding voltage; M_{em} is the electromagnetic torque and $L_{sD} = L_{sQ} = L_s$, where L_s is the stator winding inductance and L_{sD}, L_{sQ} are the d–q components of the stator winding inductance.

If the controller implements the condition, $i_{sD} = 0$, it's possible to obtain:

$$\psi_{sD} = \psi_{sf} \tag{5.6}$$

$$\psi_{sQ} = L_{sQ} \cdot i_{sQ} \tag{5.7}$$

Using the previous equations, the system's model can be summarized as follows:

$$u_{sD} = -\omega \cdot L_{sQ} \cdot i_{sQ} \tag{5.8}$$

$$u_{sQ} = R_s \cdot i_{sQ} + L_{sQ} \cdot \frac{di_{sQ}}{dt} + \omega \cdot \psi_{sf} \tag{5.9}$$

$$M_{em} = p \cdot \psi_{sf} \cdot i_{sQ} \tag{5.10}$$

The stator flux linkage equation is given by:

$$\overline{\psi_s} = \psi_{sD} + j \cdot \psi_{sQ} \tag{5.11}$$

$$\overline{\psi_s} = \psi_{sf} + j \cdot L_{sQ} \cdot i_{sQ} \tag{5.12}$$

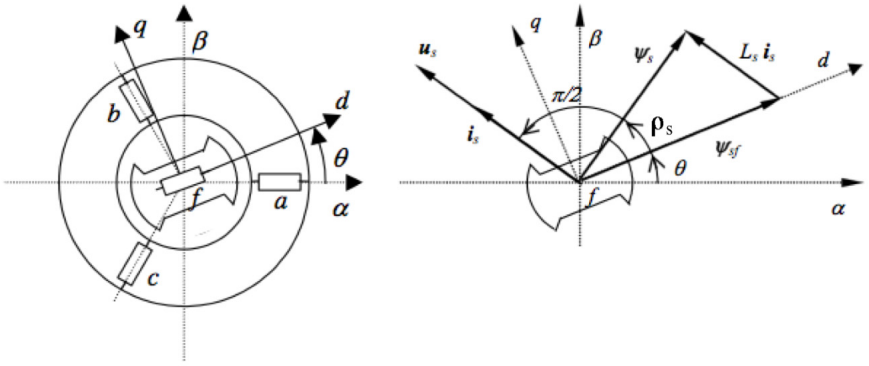

Figure 5.6. Synchronous machine control principles using the axes reference system. [20]

The stator position angle (ρ_s) can be estimated based on the flux linkages, which is obtained by the integration of electromotive force, because of the flux linkages on rotor flux reference frame includes stator position angle information.

From figure 5.6, it can be found that:

$$\sin\rho_s = \frac{\psi_{sQ}}{\psi_s} \tag{5.13}$$

Where ψ_s represents the amplitude of the stator flux linkage and ρ_s is the angle between the stator and rotor (magnet) flux linkage.

Substituting (5.13) and (5.7) into (5.10) gives:

$$M_{em} = p \cdot \frac{1}{L_s} \cdot \psi_s \cdot \psi_{sf} \cdot \sin\rho_s \tag{5.14}$$

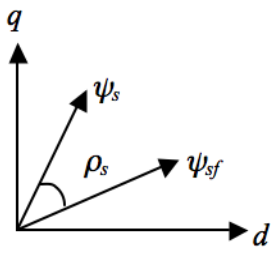

Figure 5.7. The stator and rotor flux linkage. [22]

Equation (5.14) implies that the electromagnetic torque can be controlled regulating the stator flux linkage amplitude ψ_s and the angle ρ_s. [22]

The surface mounted rotor PMSM is characterized by equal and small inductances along both the direct- and quadrature-axis, L_{sD} e L_{sQ}. Then, the stator flux, ψ_s is approximately constant (as figure 5.8 represents), and the condition $i_{sD}=0$ originates an optimal situation between the produced torque and the absorbed current.

The figure 5.8 shows the stator flux linkage variation. This flux is almost constant due to the very small inductance, L_{sQ}, which results from the machine's high magnetic air gap, because the magnets have a differential magnetic permeability similar to the air permeability.

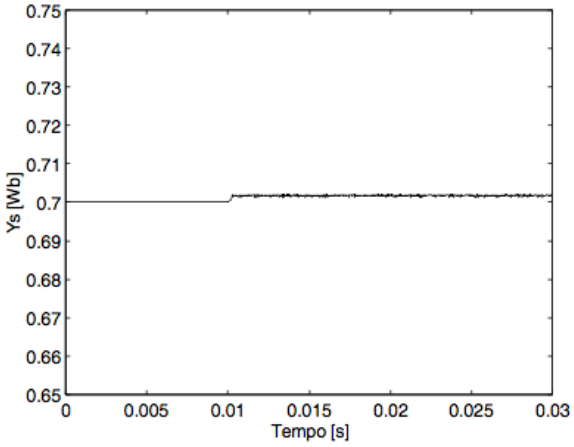

Figure 5.8. Stator flux variation. [20]

5.4 Direct Flux and Torque Control, without position sensors

The figure 5.9 represents the scheme for the Direct Flux and Torque Control.

The reference values for torque and stator flux (ψ_s^*, M_{em}^*) will be compared respectively to their estimated values and the $\Delta\psi_s$ and ΔM_{em} errors will be an input of the voltage vector selection block.

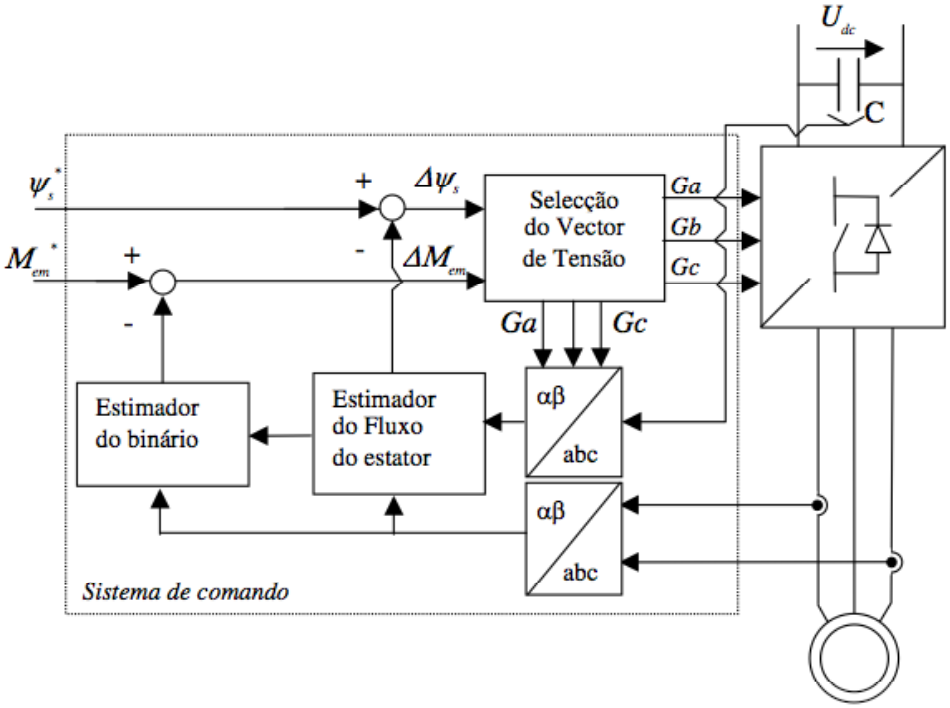

Figure 5.9. Direct Flux and Torque Control block diagram. [20]

The voltage vector selection was based on the instantaneous errors of stator flux and torque.

The scheme only uses, for monitoring, two sensors for the stator current and one sensor for the d.c. link voltage, but no position sensors. The phase voltages were obtained using the switching functions, G_a, G_b, e G_c, which are the outputs of the command system.

The figure only represents a base system, which uses, as control variables, the stator flux amplitude and the torque.

5.5 Vector control of a PMSM without sensors

To increase the robustness of the overall system it is desirable to eliminate the mechanical sensors in vector-controlled drives. For the elimination of these sensors, the next indirect sensoring techniques are well known and can easily be applied in flywheels:

1. Open-loop estimators using monitored stator voltages/currents [21];
2. Back e.m.f.-based position estimators [21];
3. Observed-based (e.g. extended Kalman filter) speed and position estimators [21];
4. Estimators using artificial intelligence [21].

The first two control techniques will be analyzed in the following sections, due to their possible application on the designed machine.

In general, when a speed and position sensorless control scheme is used, the PMSM is not self-starting, since around standstill it is difficult to estimate the stator-flux position by the estimators listed. To avoid this problem, ramp acceleration could be used as an example for starting strategy.

Similar problems exist with back e.m.f-based estimators, where the back e.m.f. can only be estimated after the motor has been first started and brought to a certain speed.

5.5.1 Vector control using open-loop flux and speed estimators using monitored stator voltages/currents

A simple position-sensorless control system is described for the vector control of a PMSM (with sinusoidal back e.m.f.) supplied by a current-controlled PWM voltage source inverter. For this purpose, in a first implementation, the monitored stator voltages and currents are used to estimate the position of the stator flux-linkage space vector through which the phase angles of the stator currents can be controlled. However, in an alternative position-sensorless scheme, only the stator currents are monitored together with the d.c. link voltage. (This allows practical implementation).

In general, for a synchronous machine in the steady-state, the first time-derivative of the angle of the stator flux-linkage space vector (ρ_s), gives exactly the rotor speed, $\omega_r = \frac{d\rho_s}{dt}$. However, in the transient state, in a drive where there is a change in the reference

electromagnetic torque, the stator flux-linkage space vector moves relative to the rotor, and this influences the rotor speed.

- *Open-loop flux estimators, voltage reconstruction, drift compensation*

The stator-flux space vector can be obtained by integration of the terminal voltage minus the stator ohmic drop:

$$\overline{\psi_s} = \int (\overline{u_s} - R_s \cdot \overline{i_s})\, dt \tag{5.15}$$

Considering:

$$\overline{u_s} = u_{sD} + j u_{sQ} \tag{5.16}$$

$$\overline{i_s} = i_{sD} + j i_{sQ} \tag{5.17}$$

$$\overline{\psi_s} = \psi_{sD} + j \psi_{sQ} \tag{5.18}$$

The angle of the stator flux-linkage space vector can be obtained from the two-axis stator flux-linkage components (as it can be concluded from figures 5.7 and 5.8):

$$\rho_s = \tan^{-1}\left(\frac{\psi_{sD}}{\psi_{sQ}}\right) \tag{5.19}$$

It is important to note that the performance of a PMSM drive depends greatly on the accuracy of the estimated stator flux-linkage components.

Drift compensation is also an important factor in the practical implementation, since it can cause large errors of the position of the stator flux-linkage space vector. In a speed control loop, this drift error will cause an undesirable fundamental frequency modulation of the modulus of the reference stator-current space vector $|\overline{i}_{sref}|$.

It should also be noted that in addition to the stator flux estimation, it is also possible

to construct another stator flux-linkage estimator, where the integration drifts are reduced at low frequency. For this purpose, instead of open-loop integrators, closed-loop integrators are introduced.

$$\overline{\psi_s} = \left|\overline{\psi_s}\right| \cdot \exp\left(j\rho_s\right) = \psi_{sD} + j\psi_{sQ} \tag{5.20}$$

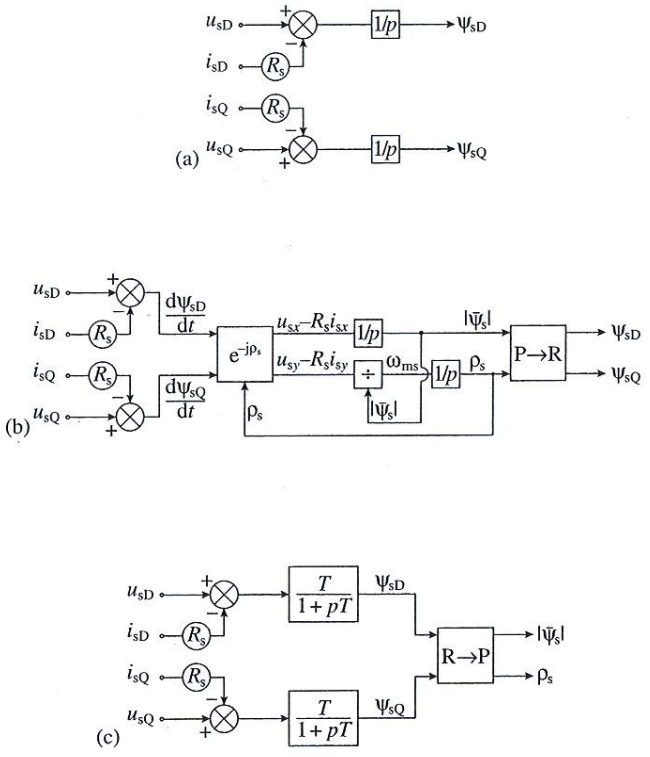

Figure 5.10. Stator flux-linkage estimators. (a) Estimation in the stationary reference frame; (b) estimation in the stator-flux-oriented reference frame; (c) estimation in the stationary reference frame using quasi-integrators. [21]

It is also possible to estimate the stator flux-linkage components by using low-pass filters instead of pure integrators. In this case $1/p$ is replaced by $T/(1+pT)$ where T is a suitable time constant.

The estimation of the stator flux-linkage components requires the stator terminal voltages. However, it is possible to have a scheme in which these voltages are not monitored, but they are reconstructed from the d.c. link voltage (U_{dc}) and the switching states (G_a, G_b, G_c) of the six switching devices of a six-step voltage-source inverter.

The stator-voltage space vector can be obtained by using the switching states and the d.c. link voltage U_{dc} [21], as:

$$\overline{u_s} = \frac{2}{3} \cdot U_{dc} \cdot \left(G_a + a \cdot G_b + a^2 \cdot G_c \right) \tag{5.21}$$

- *Inverter switches and the switching functions:*

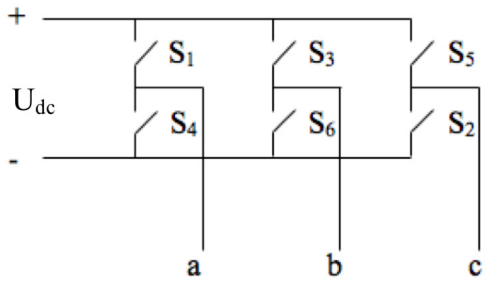

G_a=1	S_1 ON	S_4 OFF
G_a=0	S_1 OFF	S_4 ON
G_b=1	S_3 ON	S_6 OFF
G_b=0	S_3 OFF	S_6 ON
G_c=1	S_5 ON	S_2 OFF
G_c=0	S_5 OFF	S_2 ON

Due to the finite turn-off times of the switching devices (power transistors) used in a three-phase PWM VSI (voltage source inverter), there is a need to insert a time delay (dead time) after switching a switching device off and the other device on in one inverter leg. This prevents the short-circuit across both switches in the inverter leg and the d.c. link voltage.

If analog integrators are used, a source of drift is the thermal drift of these integrators and a transient offset also arises from the d.c. components which result after a transient change. Drift will cause an error in the flux position calculation. Drift compensation of the direct- and quadrature-axis stator flux-linkage components can be achieved by subtracting the respective drift flux-linkage components.

- *Rotor position estimation using stator flux linkages*

This rotor estimation technique is problematic at very low speeds (the problems are associated with the flux estimation). Parameter variations (due to saturation and temperature

effects) also influence the accuracy of the estimation. By using the determined rotor position, it is also possible to determine the rotor speed and then a drive without position and speed sensors can be implemented. For practical implementation, it is required the application of a DSP.

- *Open-loop speed estimators*

The relationship $\omega_r = \frac{d\rho_s}{dt}$ can be directly utilized in the speed control loop of the permanent-magnet synchronous motor drive.

Since the estimated value of rotor speed can be obtained by differentiation operation of the estimated rotor position angle obtained at the previous equation, a position and speed sensorless control can be attained.

However for operation at low speeds, the same limitations hold as above.

- *Stator current-controlled inverter-fed PMSM drive scheme*

In this section, a stator current-controlled inverter-fed PMSM drive control scheme is discussed, which uses an open-loop position and speed estimator. Around standstill, it is difficult to estimate the position of the stator flux-linkage space vector by the open-loop flux-linkage estimator described, since the terminal voltages minus the ohmic drops are too small. So, a ramp acceleration could be used as an example for starting strategy.

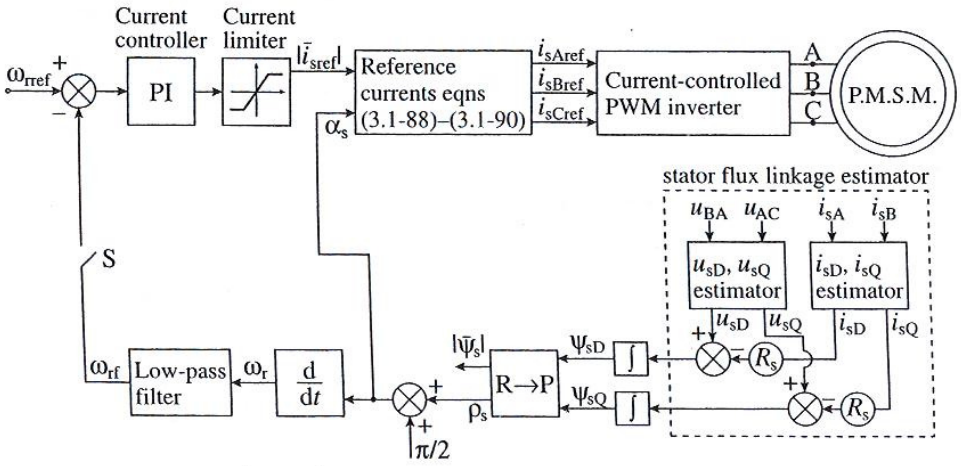

Figure 5.11. Position-sensorless vector-control of a PM synchronous machine supplied by a current-controlled PWM voltage-source inverter. [21]

The machine is supplied by a current-controlled PWM VSI, and the current controllers are hysteresis controllers. The stator flux linkages are obtained by an open-loop flux estimator. This is obtained by using the monitored values of the stator voltages and currents.

There is a speed control loop, which is the outer loop, and there is also a current loop, which is the inner loop. The speed error is fed into a PI controller. The initial acceleration is limited to ensure a small value of acceleration during starting to yield minimal speed oscillations during start-up. During start-up, the flux-linkage estimator is inactive and switch S is open, and ω_{rref} is the reference value of the ramp speed.

In the PWM-fed drive the line-to-line stator voltages change very rapidly and have high-frequency content (modulation noise). The stator currents also contain high frequency components. It follows that any differentiation used in the differentiation block would amplify these. Thus a low-pass filter is used to reduce this noise.

5.5.2 Vector control using back E.M.F.–based position estimators

In a PMSM the back e.m.f., is position dependent. Thus, if this can be accurately monitored, the rotor position can be accurately determined in real-time and this can be used to control the switching pattern of the inverter. There are four main methods:

1. The zero-crossing method, where the instant (switching point) is detected at which the back e.m.f. of an unexcited stator phase crosses zero or reaches a predetermined level (this is the simplest technique, but only suitable for steady-state operation).
2. The phase-locked loop method, where the position signals are locked on to the back e.m.f. in the unexcited stator phase during each sixty-degree interval.
3. The back e.m.f. integration method, where a switching pulse is obtained when the absolute value of the integrated back e.m.f. reaches a pre-set threshold value.
4. The indirect estimation of the back e.m.f.s by detecting the conduction interval of free-wheeling diodes connected in anti-parallel with the power transistors of the inverter.

All these methods are problematic at low speeds, but this wouldn't be a problem for the desired application, since the machine will only be used for high speeds.

The methods 1, 3 and 4 can be summarized in:

- *Application of the zero-crossing method* [21]

The zero-crossing method is the simplest, although it cannot be used in high-dynamic-performance applications, even so, this method could eventually be used in the desired application of this work (because it can be considered a steady-state application).

This method can be used to obtain equivalent rotor position information in an inverter-fed brushless d.c. motor drive (PMSM with trapezoidal m.m.f.). The zero-crossing method is based on detecting the instant where the back e.m.f. in the unexcited phase crosses zero. This zero-crossing is then used to obtain the switching sequence.

Since the back e.m.f.s are zero at zero speed, the technique cannot be used at zero speed, and the machine is not self-starting. Ideal applications for such a system are steady-state applications. Since the modulation noise is eliminated by using low-pass filters, this can cause a phase delay which is a function of the speed, and thus it is not possible to achieve optimum control, which affects the torque/ampere capability and efficiency of the motor adversely as the speed changes. Although this problem can be reduced by applying a filter phase-delay compensator, maximum performance can still not be achieved at low speeds. [21]

- *Application of the back e.m.f integration method* [21]

The back e.m.f. integration technique can be used for the detection of the rotor position of the brushless d.c. machine, which is supplied by an inverter. When this technique is used, first the phase-to-neutral voltage of the unexcited stator winding of the brushless d.c. machine is selected. This is equal to the desired back e.m.f. required for position sensing. The modulus of this back e.m.f. is integrated as soon as the back e.m.f. crosses zero. When the integrated voltage reaches a pre-set threshold value, the next switching instant occurs.

The integrator has also the advantage of reducing the switching noises. Furthermore, since the back e.m.f. amplitude is proportional to the speed, the conduction intervals automatically scale inversely with the speed, so there is an automatic adjustment of the inverter switching to change the speed.

Similarly to other back-e.m.f.-based control schemes, accuracy problems arise at low speed and in addition the machine is not self-starting. Control of the motor currents is important in a high-dynamic-performance drive, since this provides the basis for instantaneous torque control. It is possible to utilize the back e.m.f. integration method in a drive to have high quality current and instantaneous torque control in all operating modes.

- *Application of the indirect estimation of the back e.m.f.s by detecting the conducting interval of free-wheeling diodes* [21]

Indirect position estimation of the back e.m.f.s can be based on detecting the conduction state of the free-wheeling diodes in the unexcited stator phase of a brushless d.c.

machine. The approach can be used over a wide speed-range, even at very low speeds (but not zero speed). The free-wheeling diodes are connected in anti-parallel with the power transistors, and provide a current flow path to dissipate inductive energy stored in a winding.

Since the amplitude of the back e.m.f. is proportional to the rotor speed, similarly to the other back-e.m.f.-based techniques, the motor is not self-starting and a special starting technique must be applied. On the other hand, it is an advantage that it allows the detection of the position at very low speeds as well, but the technique requires the inverter to operate in the chopping mode.

5.6 Conclusions

This chapter reports one of the main goals of this work: the machine sensorless control.

A sensorless control is desirable instead of using mechanical sensors, in order to reduce total hardware complexity, size, cost and maintenance requirements.

After a study of the sensorless control methods, the Direct Flux and Torque Control was the chosen technique to control the system, due to its efficiency and simplicity.

Chapter 6

Conclusions

This chapter finalises this work, presenting conclusions and pointing out aspects to be developed in future work.

The current thesis intended to be a preliminary design of an electrical machine (and its control) for application at a flywheel energy-storage system, for possible use at road vehicles.

The chosen flywheel's rotor materials were the carbon-based fibers, which stores more energy per volume, comparing to iron and other classical materials. A study of the stress forces variation along the rotor was performed, which permitted to conclude that the tangential stress is more limitative than the radial stress.

The flywheel's rotor dimensions were related to the rotation speed, the cylinder weight and the material's cost. Based on those relations, it was concluded that a flywheel energy-storage system with 5 kWh capacity could be designed for application on an electric vehicle, having two robust rotors of 2,5 kWh and 44 Kg, each one. The two rotors material's cost will be around $3000.

The transformation between rotational kinetic energy and electrical energy was performed with two permanent magnet synchronous machine (motor/generator) of 30 kW (40,23 hp) each. The permanent magnet synchronous machine was chosen due to its efficiency, smaller size and easier control, when compared to direct current machines or induction machines.

The calculated machine dimensions were related to the kinetic energy stored, concluding that the energy increases directly proportional with L and inversely proportional with D.

After the calculations for the machine design, it was studied a sensorless control system appropriate for this machine.

It was desirable a sensorless control instead of using mechanical sensors, in order to reduce total hardware complexity, size, cost and maintenance requirements. Due to its efficiency and simplicity, the Direct Flux and Torque Control, was the chosen technique.

NASA projected some developments in future work, for flywheels application, which are listed in the figure 6.1.

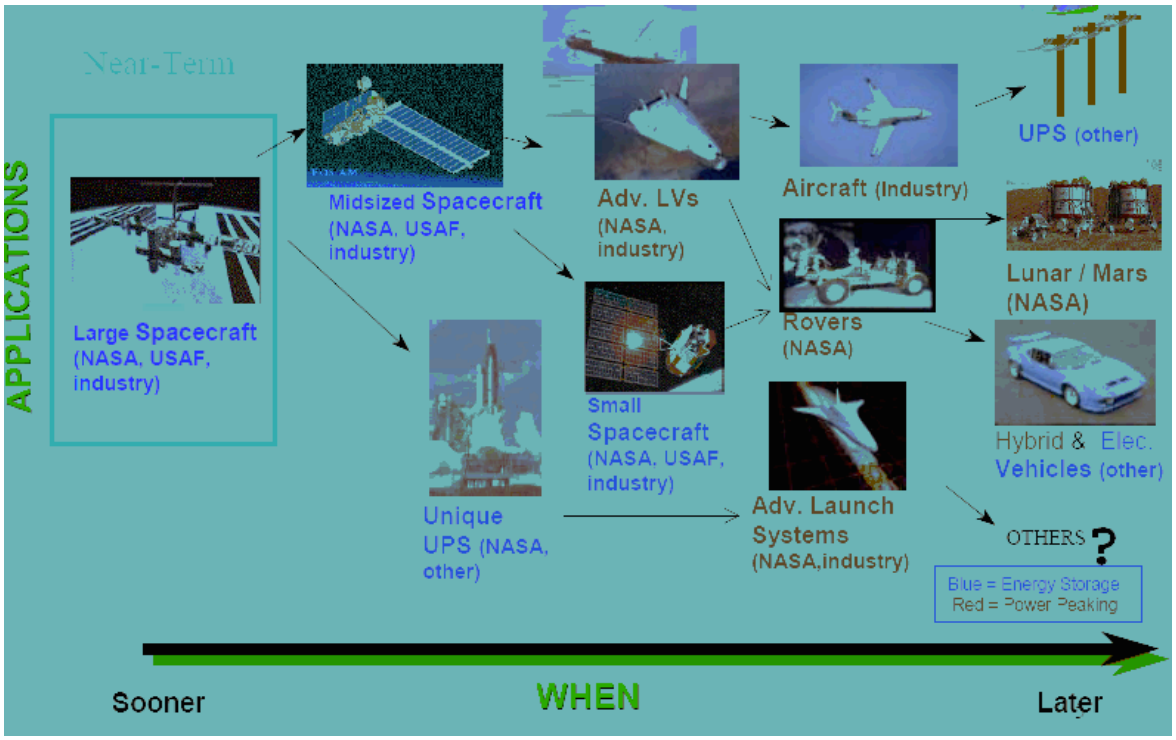

Figure 6.1. NASA's intended future work for flywheel's applications. [12]

Possible future developments of the work described in this thesis, could be the practical implementation of the chosen control system, the construction of the designed flywheel and the posterior application of the designed machine at this flywheel.

Annex 1

Poisson's Ratio

Poisson's ratio is a physical constant of materials, defined by the ratio of lateral strain and axial strain and can be expressed by the next figure and equation:

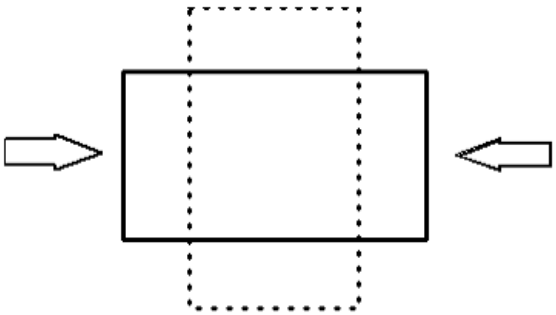

Figure A1.1. Material stretched in one direction. [29]

$$\nu = -\frac{\varepsilon_{yy}}{\varepsilon_{xx}} \tag{A.1}$$

Where ε_{yy} is the transverse strain and ε_{xx} is the longitudinal or axial strain.

The Poisson ratio for most metals falls between 0.25 to 0.35 [30]. Rubber has a Poisson ratio close to 0.5 and is therefore almost incompressible. Theoretical materials with a Poisson ratio of exactly 0.5 are truly incompressible, since the sum of all their strains leads to a zero volume change. Cork, on the other hand, has a Poisson ratio close to zero.

The Poisson's ratio is bounded by two theoretical limits, it must be greater than -1 and less than or equal to 0.5:

$$-1 < \nu \leq \frac{1}{2} \tag{A.2}$$

However, it is rare to encounter engineering materials with negative Poisson ratios. Most materials will fall in the range,

$$0 \leq \nu \leq \frac{1}{2} \tag{A.3}$$

According to [28], the Poisson’s ratio for resin-bounded woven carbon fibers is 0.3.

Annex 2

Calculations of a flywheel rotor's dimensions for different energy capacities

For the design of the flywheel, carbon AS4C was the chosen material, which density is $\rho = 1510 Kg/m^3$.

The maximum tensile strength for this material is 1650 MPa. For the σ_t it will be used half of the material's maximum value, as a security factor.

$$\sigma_t = \frac{1650}{2} MPa = 825 MPa$$

For the inner and outer radius relation, $\frac{r_i}{r_o} = \frac{\sqrt{2}}{2}$ was achieved and for the height and outer radius relation, $h = 2 \cdot r_o$ was chosen (for size limitations).

$$\frac{r_i}{r_o} = \frac{\sqrt{2}}{2} \Rightarrow \left(\frac{r_i}{r_o}\right)^4 = \frac{1}{4}$$

$$h = 2 \cdot r_o$$

Using equation (2.13), the next simplification can be concluded:

$$E_{\lim} = \frac{1}{4} \cdot \pi \cdot h \cdot \left(1 - \left(\frac{r_i}{r_o}\right)^4\right) \cdot r_o^2 \cdot \sigma_t \Rightarrow E_{\lim} = \frac{3}{16} \cdot \pi \cdot h \cdot r_o^2 \cdot \sigma_t \Rightarrow E_{\lim} = \frac{3}{8} \cdot \pi \cdot r_o^3 \cdot \sigma_t$$

For the linear speed and tensile strength relation, the next equation will be used:

$$\frac{\sigma_t}{\rho \cdot \omega^2 \cdot r_o^2} \approx 1$$

- *1st series of calculations (with σ_t=825MPa)*

For this 1st series, the energy of the flywheel was fixed and the dimension and speed of the wheel were calculated.

Calculation of rotor's dimensions for $E_{\lim} = 2.5 kWh = 9 MJ$:

$$E_{\lim} = \frac{3}{8} \cdot \pi \cdot r_o^3 \cdot \sigma_t \Rightarrow 9 \times 10^6 = \frac{3}{8} \cdot \pi \cdot r_o^3 \cdot 825 \times 10^6 \Rightarrow r_o = 0.21m$$

$$h = 2 \cdot r_o = 2 \times 0.21 = 0.42m$$

$$\frac{r_i}{r_o} = \frac{\sqrt{2}}{2} \Rightarrow r_i = 0.148m$$

Calculation of angular velocity for $r_o = 0.21m$:

$$\frac{\sigma_t}{\rho \cdot \omega^2 \cdot r_o^2} = 1 \Rightarrow \omega^2 = \frac{825 \times 10^6}{1510 \times 0.21^2} \Rightarrow \omega = 3519.95 rad/s = 33613 rpm$$

The calculation of rotors' dimensions for $E_{\lim} = 1kWh = 3.6MJ$ and $E_{\lim} = 25kWh = 90MJ$ were made, using the same procedure as before, but with different values of energy. The results can be seen in table 2.3.

- *2nd series of calculations (with σ_t=825MPa)*

In this series, the maximum speed of the wheel was fixed and the wheel's dimensions and energy calculated.

Calculation of rotor's dimensions for $\omega = 60000 rpm = 6283.19 rad/s$

$$\frac{\sigma_t}{\rho \cdot \omega^2 \cdot r_o^2} = 1 \Rightarrow r_o^2 = \frac{825 \times 10^6}{1510 \times 6283.19^2} \Rightarrow r_o = 0.118m$$

$$h = 2 \cdot r_o = 2 \times 0.118 = 0.235m$$

$$\frac{r_i}{r_o} = \frac{\sqrt{2}}{2} \Rightarrow r_i = 0.083m$$

Calculation of the stored energy for $r_o = 0.118m$:

$$E_{\lim} = \frac{3}{8} \cdot \pi \cdot r_o^3 \cdot \sigma_t \Rightarrow E_{\lim} = \frac{3}{8} \cdot \pi \cdot 0.118^3 \cdot 825 \times 10^6 = 1.58MJ = 0.441kWh$$

- *3rd series of calculations (with σ_t=825MPa)*

This calculations intended to test safe limits. Certain energy and speed limits were specified, being the size and the tensile strength calculated for the specified values.

Calculation of rotor's dimensions for $E_{\lim} = 2.5kWh = 9MJ$; $\omega = 60000rpm =$ $= 6283.19rad/s$:

$$\frac{\sigma_t}{\rho \cdot \omega^2 \cdot r_o^2} = 1 \Leftrightarrow \sigma_t = \rho \cdot \omega^2 \cdot r_o^2$$

$$E_{\lim} = \frac{1}{4} \cdot \pi \cdot h \cdot \left(1 - \left(\frac{r_i}{r_o}\right)^4\right) \cdot r_o^2 \cdot \sigma_t \Rightarrow E_{\lim} = \frac{1}{4} \cdot \pi \cdot h \cdot \left(1 - \left(\frac{r_i}{r_o}\right)^4\right) \cdot r_o^4 \cdot \rho \cdot \omega^2 = \frac{3}{16} \cdot \pi \cdot h \cdot r_o^4 \cdot \rho \cdot \omega^2$$

$$E_{\lim} = \frac{3}{8} \cdot \pi \cdot r_o^5 \cdot \rho \cdot \omega^2 \Rightarrow 9 \times 10^6 = \frac{3}{8} \cdot \pi \cdot r_o^5 \cdot 1510 \cdot 6283.19^2 \Rightarrow r_o = 0.167m$$

$$h = 2 \cdot r_o = 2 \times 0.167 = 0.333m$$

$$\frac{r_i}{r_o} = \frac{\sqrt{2}}{2} \Rightarrow r_i = 0.118m$$

Calculation of the tensile strength for $r_o = 0.167m$:

$$\sigma_t = \rho \cdot \omega^2 \cdot r_o^2 \Rightarrow \sigma_t = 1653.59MPa$$

This value is superior to the maximum admitted for the material.

The problem of this calculation is that the σ_t is not limited.

- *4th calculations (with σ_t=825MPa)*

Supposing $h = 4 \cdot r_o$, instead of $h = 2 \cdot r_o$ and using the method developed in the first calculations, the calculation of rotor's dimensions for $E_{\lim} = 2.5kWh = 9MJ$ is:

$$E_{\lim} = \frac{1}{4} \cdot \pi \cdot h \cdot \left(1 - \left(\frac{r_i}{r_o}\right)^4\right) \cdot r_o^2 \cdot \sigma_t \Rightarrow E_{\lim} = \frac{3}{16} \cdot \pi \cdot h \cdot r_o^2 \cdot \sigma_t \Rightarrow E_{\lim} = \frac{3}{4} \cdot \pi \cdot r_o^3 \cdot \sigma_t$$

$$E_{\lim} = \frac{3}{4} \cdot \pi \cdot r_o^3 \cdot \sigma_t \Rightarrow 9 \times 10^6 = \frac{3}{4} \cdot \pi \cdot r_o^3 \cdot 825 \times 10^6 \Rightarrow r_o = 0.167m$$

$$h = 4 \cdot r_o = 4 \times 0.167 = 0.667m$$

$$\frac{r_i}{r_o} = \frac{\sqrt{2}}{2} \Rightarrow r_i = 0.118m$$

Calculation of angular velocity for $r_o = 0.167m$:

$$\frac{\sigma_t}{\rho \cdot \omega^2 \cdot r_o^2} = 1 \Rightarrow \omega^2 = \frac{825 \times 10^6}{1510 \times 0.167^2} \Rightarrow \omega = 4434.85rad/s = 42350rpm$$

Annex 3

Calculation of Machine Dimensions D_{in} and L

The main dimensions D_{in} and L can be determined, using the output equation (4.10), for a determined power rating of the machine.

The following parameters were used for the calculations in an illustrating example:

$P_{kW} = 30kW$ (This value was fixed)

$p = 2$ (This value was fixed)

$N = \frac{N_{\max}}{2} = \frac{33613}{2} = 16806.5rpm \approx 15000rpm$ (N_{max} obtained from Chapter 2)

$f = \frac{p \cdot N}{120} = \frac{2 \cdot 15000}{120} = 250Hz$

$B_{gav} = 0.6Wb/m^2$ (In order to obtain a working point near the BH_{max})

$K_w = 0.966$

$A = 20000ampere - conductors/m$

$\cos\varphi = 1$ (This value is a characteristic of the synchronous machine)

$\eta = 95\%$ (Common efficiency for a machine of this type)

The next three series of calculations represent three different results for D_{in} and L, and the best result will be chosen.

- 1st – Using the aspect ratio $\frac{L}{\tau} = 1.00 \Rightarrow L = \frac{\pi \cdot D_{in}}{4}$ (usually applied to low speed machines):

$$D_{in}^{\ 2} \cdot L = \frac{5480}{A \cdot B_{gav} \cdot K_w \cdot \cos\varphi \cdot \eta \cdot N} \cdot P_{kW}$$

$$L = \frac{\pi \cdot D_{in}}{4}$$

The previous equations results in:

$$D_{in}{}^{3} = \frac{5480 \cdot 4}{A \cdot B_{gav} \cdot K_w \cdot \cos\varphi \cdot \eta \cdot N \cdot \pi} \cdot P_{kW} \Rightarrow D_{in} = 0.1082m$$

$$L = \frac{\pi \cdot D_{in}}{4} = 0.0850m$$

- 2nd – Using the aspect ratio $\frac{L}{\tau} = 4.00 \Rightarrow L = \frac{\pi \cdot D_{in}}{1}$ (usually applied to high speed machines):

$$D_{in}{}^{2} \cdot L = \frac{5480}{A \cdot B_{gav} \cdot K_w \cdot \cos\varphi \cdot \eta \cdot N} \cdot P_{kW}$$

$$L = \frac{\pi \cdot D_{in}}{1}$$

The previous equations results in:

$$D_{in}{}^{3} = \frac{5480 \cdot 1}{A \cdot B_{gav} \cdot K_w \cdot \cos\varphi \cdot \eta \cdot N \cdot \pi} \cdot P_{kW} \Rightarrow D_{in} = 0.0682m$$

$$L = \frac{\pi \cdot D_{in}}{1} = 0.2142m$$

- 3rd – Supposing now, that L will be a fixed parameter (near the maximum height admitted, 0.42m). With $L = 0.4m$:

$$D_{in}{}^{2} \cdot L = \frac{5480}{A \cdot B_{gav} \cdot K_w \cdot \cos\varphi \cdot \eta \cdot N} \cdot P_{kW} \Rightarrow D_{in}{}^{2} = \frac{5480}{A \cdot B_{gav} \cdot K_w \cdot \cos\varphi \cdot \eta \cdot N \cdot L} \cdot P_{kW} \Rightarrow$$

$$\Rightarrow D_{in} = 0.0499m$$

Annex 4

Relation Between the Machine Parameters E_{ph}, L and D_{in}

A4 1. Relation between $E_{ph\ per\ spire}$ and L, with $D=0.0682m$

Using equation (4.3), which represents E_{ph}, it was possible to obtain the equation of E_{ph} per spire:

$$E_{ph} = 4.44 \cdot \left(\frac{p \cdot N}{120}\right) \cdot K_w \cdot N_{ph} \cdot \left(B_{gav} \cdot \pi \cdot \frac{D \cdot L}{p}\right) \Rightarrow$$

$$\Rightarrow E_{ph\_per\_spire} = 4.44 \cdot \left(\frac{p \cdot N}{120}\right) \cdot K_w \cdot \left(B_{gav} \cdot \pi \cdot \frac{D \cdot L}{p}\right)$$

The next graphic shows $E_{ph\_per\_spire}$ for different values of L, supposing $D = 0.0682m$ (which is the equivalent value for $L = 0.2142m$, obtained at 4.3, 2nd series of calculations).

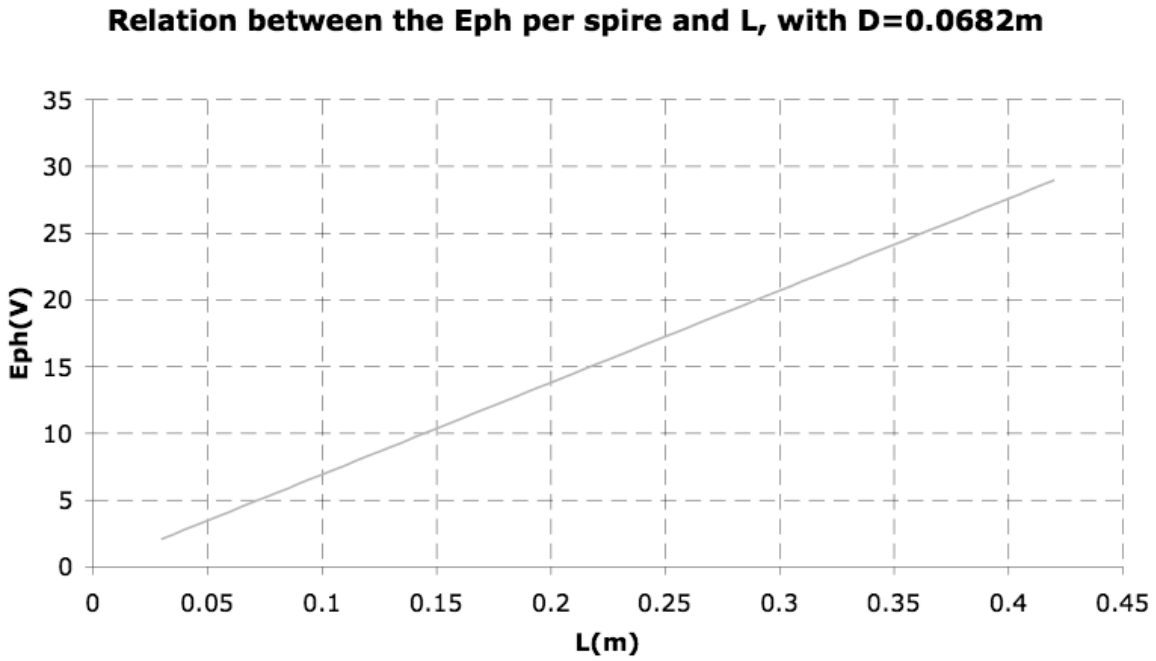

Figure A4.1. Relation between Eph per spire and L, with D=0.0682m

$$L = 0.2142m \Rightarrow E_{ph\_per\_spire} \approx 14.75V$$

As it was expected by the analysis of the equations, the graphic shows that $E_{ph\_per\_spire}$ grows in order to L, for a fixed D.

A4 2. Relation between $E_{ph\ per\ spire}$ and L

Using equation (4.10) in equation (4.3), it was possible to obtain the relation only between $E_{ph\_per\_spire}$ and L:

$$D^2 \cdot L = \frac{5480}{A \cdot B_{gav} \cdot K_w \cdot \cos\varphi \cdot \eta \cdot N} \cdot P \Rightarrow D = \sqrt{\frac{5480}{A \cdot B_{gav} \cdot K_w \cdot \cos\varphi \cdot \eta \cdot N \cdot L} \cdot P}$$

$$E_{ph} = 4.44 \cdot \left(\frac{p \cdot N}{120}\right) \cdot K_w \cdot N_{ph} \cdot \left(B_{gav} \cdot \pi \cdot \frac{D \cdot L}{p}\right) \Rightarrow$$

$$\Rightarrow E_{ph\_per\_spire} = 4.44 \cdot \left(\frac{p \cdot N}{120}\right) \cdot K_w \cdot \left(B_{gav} \cdot \pi \cdot \frac{D \cdot L}{p}\right)$$

The next graphic shows $E_{ph\_per\_spire}$ for different values of L.

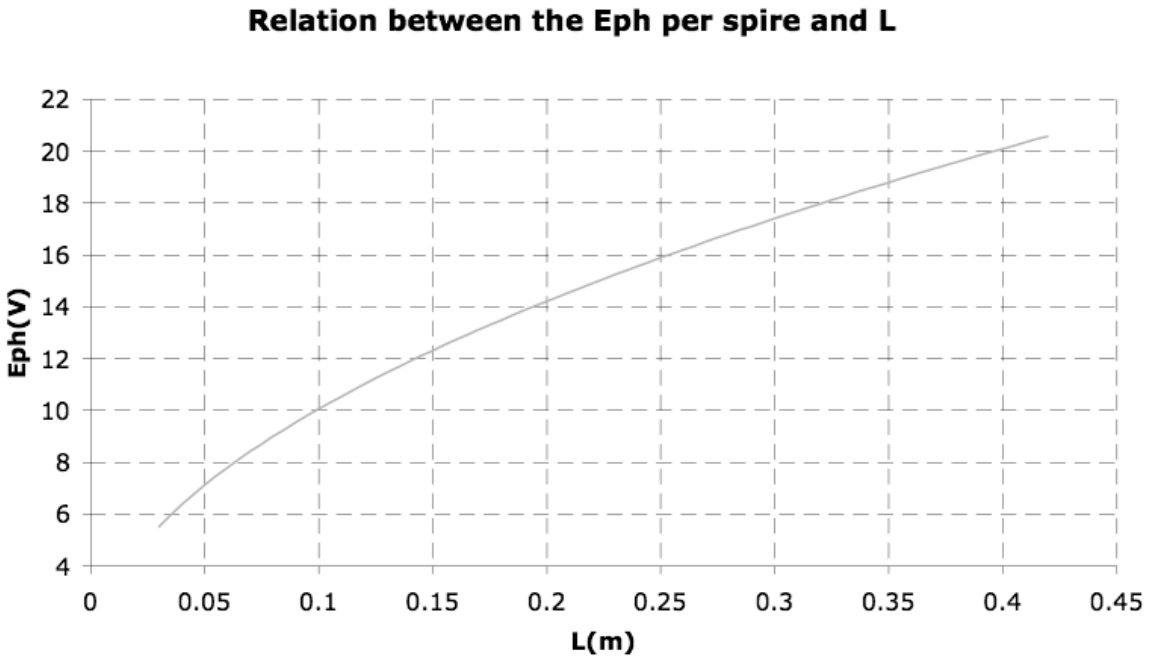

Figure A4.2. Relation between $E_{ph\ per\ spire}$ and L

$$L = 0.2142m \Rightarrow E_{ph\_per\_spire} \approx 14.75V$$

As it was expected by the analysis of the equations, the graphic shows that $E_{ph\_per\_spire}$ grows in order to $\sqrt{L}$.

A4 3. Relation between E_{ph} and L

Similarly to the previous calculation, using equation (4.10) in equation (4.3), it was obtained the relation only between E_{ph} and L:

$$D^2 \cdot L = \frac{5480}{A \cdot B_{gav} \cdot K_w \cdot \cos\varphi \cdot \eta \cdot N} \cdot P \Rightarrow D = \sqrt{\frac{5480}{A \cdot B_{gav} \cdot K_w \cdot \cos\varphi \cdot \eta \cdot N \cdot L} \cdot P}$$

$$E_{ph} = 4.44 \cdot \left(\frac{p \cdot N}{120}\right) \cdot K_w \cdot N_{ph} \cdot \left(B_{gav} \cdot \pi \cdot \frac{D \cdot L}{p}\right)$$

Using $N_{ph} = 68$ (obtained at 4.6) at the above equation, it was possible to obtain the next graphic, which shows E_{ph} for different values of L.

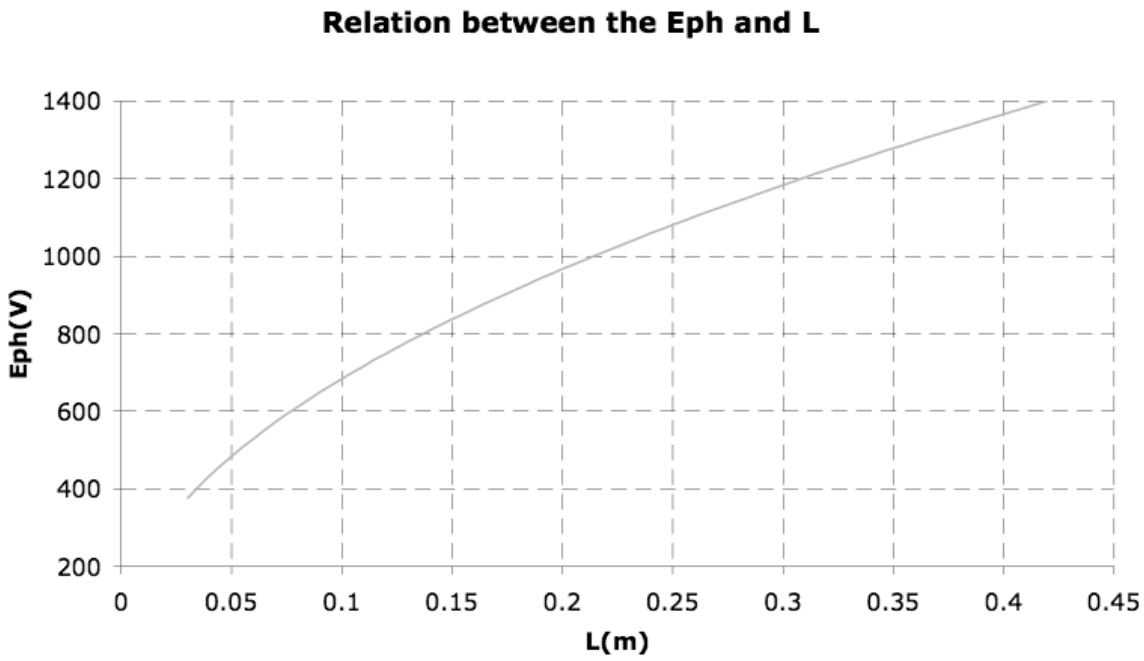

Figure A4.3. Relation between E_{ph} and L

$$L = 0.2142m \Rightarrow E_{ph} \approx 1000V$$

The value of E_{ph} for this L was the expected, because it was specified to this value for the calculation of N_{ph}, at 4.6. Similarly to the previous graphic, it was expected by the analysis of the equations that $E_{ph\_per\_spire}$ grows in order to $\sqrt{L}$.

A4 4. Relation between D and L

Using equation (4.10):

$$D^2 \cdot L = \frac{5480}{A \cdot B_{gav} \cdot K_w \cdot \cos\varphi \cdot \eta \cdot N} \cdot P \Rightarrow D = \sqrt{\frac{5480}{A \cdot B_{gav} \cdot K_w \cdot \cos\varphi \cdot \eta \cdot N \cdot L} \cdot P}$$

It was possible to achieve the next graphic that shows D for different values of L.

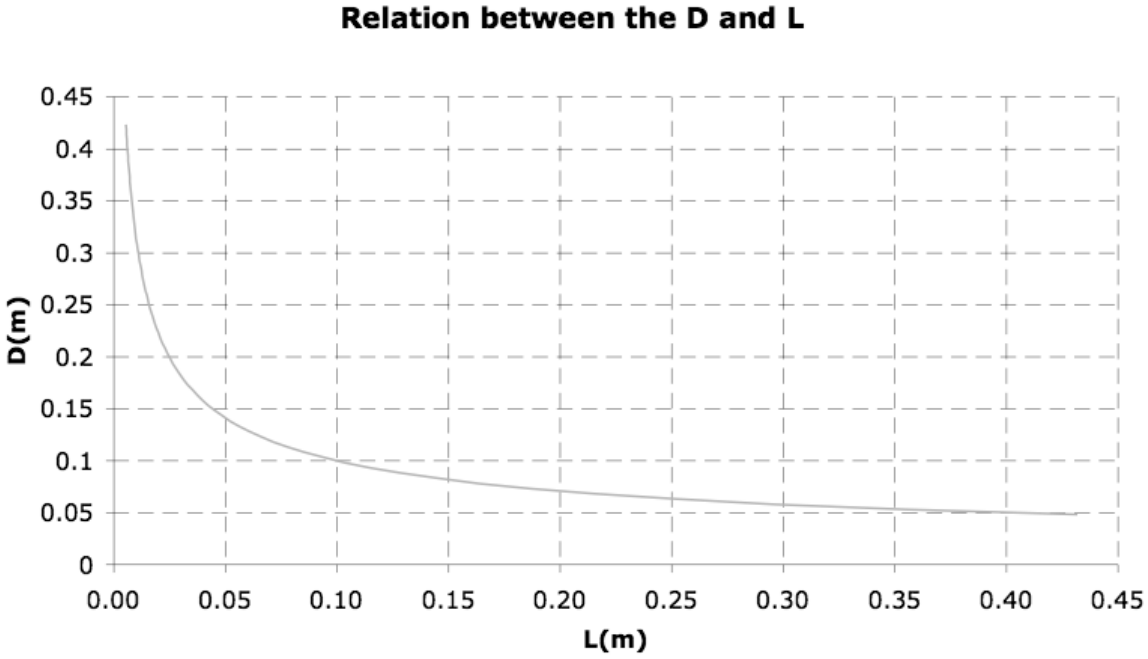

Figure A4.4. Relation between D and L

$$L = 0.2142m \Rightarrow D = 0.0682m$$

These values were obtained at 4.3, 2nd series of calculations, for the determined power rating of 30kW.

A4 5. Relation between $E_{ph\ per\ spire}$ and D

Using equation (4.10) in equation (4.3), it was possible to obtain the relation only

between $E_{ph\_per\_spire}$ and D:

$$D^2 \cdot L = \frac{5480}{A \cdot B_{gav} \cdot K_w \cdot \cos\varphi \cdot \eta \cdot N} \cdot P \Rightarrow D = \sqrt{\frac{5480}{A \cdot B_{gav} \cdot K_w \cdot \cos\varphi \cdot \eta \cdot N \cdot L} \cdot P}$$

$$E_{ph} = 4.44 \cdot \left(\frac{p \cdot N}{120}\right) \cdot K_w \cdot N_{ph} \cdot \left(B_{gav} \cdot \pi \cdot \frac{D \cdot L}{p}\right) \Rightarrow$$

$$\Rightarrow E_{ph\_per\_spire} = 4.44 \cdot \left(\frac{p \cdot N}{120}\right) \cdot K_w \cdot \left(B_{gav} \cdot \pi \cdot \frac{D \cdot L}{p}\right)$$

The next graphic shows $E_{ph\_per\_spire}$ for different values of D.

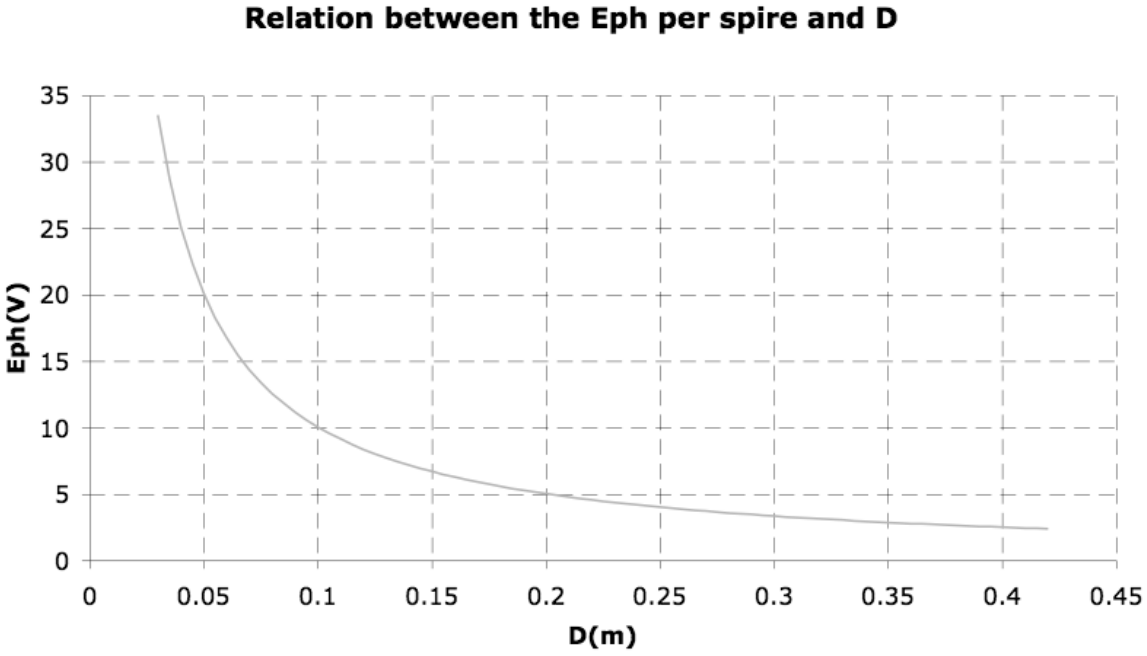

Figure A4.5. Relation between $E_{ph\ per\ spire}$ and D

$$D = 0.0682m \Rightarrow E_{ph\_per\_spire} \approx 14.75V$$

The value of $E_{ph\_per\_spire}$ for this D was the expected, because the same value was obtained in figures A4.1 and A4.2, for $L = 0.2142m$ (which is equivalent to $D = 0.0682m$).

As it was expected by the analysis of the equations, the graphic shows that $E_{ph\_per\_spire}$ grows in order to $\frac{1}{D}$.

References

[1] Hoolboom, Gerard J.; Szabados, Bama; "Nonpolluting Automobiles", *IEEE Transactions on Vehicular Technology*, vol. 43, no. 4, pp 1136-1144, November 1994.

[2] Kenny, Barbara H.; Jansen, Ralph; Kaskak, Peter; Dever, Timothy; Santiago, Walter; "Integrated Power and Attitude Control with Two Flywheels", IEEE Log No. T-AES/41/4/860803, April 2005.

[3] Strasik, M.; Johnson, P. E.; Day, A. C.; Mittleider, J.; Higgins, M. D.; Edwards, J.; Schindler, J. R.; McCrary, K. E.; McIver, C. R.; Carlson, D.; Gonder, J. F.; Hull, J. R.; "Design, Fabrication, and Test of a 5-kWh/100-kW Flywheel Energy Storage Utilizing a High-Temperature Superconducting Bearing", *IEEE Trans. Appl. Supercond.*, vol. 17, no. 2, pp 2133–2137, June 2007.

[4] Werfel, Frank N.; Floegel-Delor, Uta; Riedel, Thomas; Rothfeld, Rolf; Wippich, Dieter; Goebel, Bernd; Reiner, Gerhard; Wehlau, Niels; "A Compact HTS 5 kWh/250 kW Flywheel Energy Storage System", *IEEE Trans. Appl. Supercond.*.

[5] Bolund, Bjorn; Bernhoff, Hans; Leijon, Mats; "Flywheel Energy and Power Storage Systems", *Renewable and Sustainable Energy Reviews 11*, pp 235–258, 2007.

[6] Schweitzer, G.; "Active Magnetic Bearings – Chances and Limitations", International Center for Magnetic Bearings, ETH Zurich, CH–8092 Zurich.

[7] Mulcahy, Thomas M.; Hull, John R.; Uherka, Kenneth L.; Abboud, Robert G.; Juna, John J.; "Test Results of 2-kWh Flywheel Using Passive PM and HTS Bearings", *IEEE Transactions on Applied Superconductivity*, vol. 11, no. 1, pp. 1729–1732, March 2001.

[8] Hull, John R.; Day, Arthur C.; "Development of Flywheel Energy System",

Washington DC, July 18, 2002.

[9] Senjyu, Tomonobu; Shingaki, Takeshi; Uezato, Katsumi; "Sensorless Vector Control of Synchronous Reluctance Motors with Disturbance Torque Observer", University of the Ryukyus, Okinawa, Japan, IEEE, pp. 381–386, 2000.

[10] Senjyu, Tomonobu; Tamakia, Satoshi; Muhandoa, Endusa; Urasakia, Naomitsu; Kinjoa, Hiroshi; Funabashib, Toshihisa; Fujitac, Hideki; Sekinea, Hideomi; "Wind Velocity and Rotor Position Sensorless Maximum Power Point Tracking Control for Wind Generation System", Japan, *Renewable Energy*, nº 31, pp. 1764–1775, 2006.

[11] Song, Zhengqiang; Hou, Zhijian; Jiang, Chuanwen; Wei, Xuehao; "Sensorless Control of Surface Permanent Magnet Synchronous Motor Using a New Method", Department of Electrical Engineering, Shanghai Jiao Tong University, Shanghai, China, *Energy Conversion and Management*, nº47, pp. 2451–2460, 2006.

[12] McLallin, Kerry; "NASA Flywheel System Development", Glenn Research Center, NASA, USA, Space Power Workshop, April 4, 2001.

http://space-power.grc.nasa.gov/ppo/projects/flywheel/papers/NASA_Flywheel _S ystem_Development_SPW01.pdf

[13] Bitterly, Jack G.; "Flywheel Technology Past, Present, and 21St Century Projections", US Flywheel Systems, *IEEE AES Systems Magazine*, 0885-8985/98, pp. 13–16, August 1998.

[14] Tsukamoto, O.; Utsunomiya, A.; "HTS Flywheel Energy Storage System with Rotor Shaft Stabilized by Feed-Back Control of Armature Currents of Motor-Generator", Tsukamoto Laboratory, Faculty of Engineering, Yokohama National University, Yokohama, Japan; *Physica C: Superconductivity*, vol. 463–465, pp. 1267–1270, 2007.

[15] Nagaya, S.; Kashima, N.; Kawashima, H.; Kakiuchi, Y.; Hoshino, A.; Isobe, S.; "Development of the Axial Gap Type Motor/Generator for the Flywheel with Superconducting Magnetic Bearings", Japan, *Physica C*, vol. 392–396, pp. 764–768, 2003.

[16] Tsao, Perry; Senesky, Matthew; Sanders, Seth; "A Synchronous Homopolar Machine for High-Speed Applications", Department of Electrical Engineering, University of California, Berkeley, CA, IEEE, 0-7803-7420-7/02, pp. 406–414, 2002.

[17] Toliyat, Hamid A.; Kliman, Gerald B.; "Handbook of Electric Motors – Second Edition, Revised and Expanded", ISBN: 0-8247-4105-6, Marcel Dekker Inc., United States of America, 2004.

[18] Kostenko, M.; Piotrovski, L.; "Máquinas Eléctricas – Máquinas de Corrente Alternada" volume II, Edições Lopes da Silva, Porto, 1979.

[19] Boldea, Ion; A.Nasar, Syed; "The Induction Machine Handbook", ISBN: 0-8493-0004-5, CRC Press, 2002.

[20] Marques, Gil; "Controlo de Motores Eléctricos", Textos de apoio à disciplina de Accionamento de Veículos Eléctricos, Fevereiro 2006.

[21] Vas, Peter; "Sensorless Vector and Direct Torque Control", Oxford University Press, Inc., New York, 1998.

[22] Llor, A. M.; Rétif, J. M.; Lin-Shi, X.; Arnalte, S.; "Direct Stator Flux Linkage Control Technique for a Permanent Magnet Synchronous Machine", CEGELY-INSA, Villeurbanne, France, *Power Electronics Specialist Conference, 2003 (PESC '03)* IEEE 34th Annual; ISBN: 0-7803-7754-0; 2003.

[23] Hebner, Robert; Beno, Joseph; Walls, Alan; "Flywheel Batteries Come Around Again", University of Texas, *IEEE Spectrum*, April 2002.

[24] Schouleur, Adrien; Sapin, Julien; Kluyskens, Virginie; Labrique, Francis; Dehez, Bruno; "Study and Control of a Magnetic Bearing for Flywheel Energy Storage System", Universite Catholique de Louvain, Louvain-la-Neuve, *POWERENG 2007*, IEEE, 1-4244-0895-4/07, pp. 134–139, 2007.

[25] 1.5 kW Electromechanical battery system flywheel energy systems Inc. CETC-0100-01 Rev. 2.

[26] MS-196. Project all electric vehicle (AEV). RTP 16.02 inom WEAG. Technical

Report No. 1; Nov–Dec 2001.

[27] Taylor, P.; Johnsson, L.; Reichert, K.; DiPietro, P.; Philip, J.; Butler, P.; "A summary of the state of the art of superconducting magnetic energy storage systems, flywheel energy storage systems and compressed air energy storage systems", SAND99-1854, unlimited release; Albuquerque, New Mexico 87185 and Livermore, California 94550: Sandia National Laboratory; 1999.

[28] Mowry, Steve; "Assessing High-Performance Diaphragm Materials", Voice Coil, *The Periodical for the Loudspeaker Industry*, 2006.

[29] http://www.engineeringtoolbox.com/poissons-ratio-d_1224.html

[30] Budynas, Richard G.; Nisbett, J. Keith; "Shigley's Mechanical Engineering Design", Eight Edition, ISBN 978-007-125763-3, McGraw–Hill, October 25, 2006.

[31] Sørensen, Bent; "Renewable Energy Conversion, Transmission and Storage", ISBN 978-0123742629, Academic Press, November 1, 2007.

[32] Cimuca, Gabriel–Octavian; "Systeme Inertiel de Stockage d'Energie Associe a des Generateurs Eoliens",Ph.D. thesis, Ecole Nationale Supérieur d'Arts et Métiers, Centre de Lille, France, 2005.

[33] Bolund, Bjorn; "Electric Power Generation and Storage Using a High Voltage Approach", Digital Comprehensive Summaries of Uppsala Dissertations from the Faculty of Science and Technology 173, ISBN 91-554-6552-8, Uppsala, 2006.

[34] Lipo, T. A.; "Introduction to AC Machine Design", Vol.1, University of Wisconsin, Madison Wisconsin, USA, 1996.

[35] Sahin, F.; Tuckey, A. M.; Vandenput, A. J. A.; "Design, development and testing of a high-speed axial-flux permanent-magnet machine"; IEEE, 0-7803-7116-X/01, pp. 1640–1647, 2001.